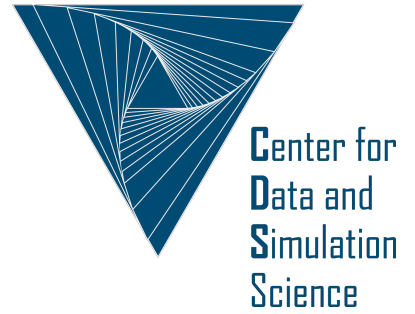


Universität
zu Köln



Technical Report Series Center for Data and Simulation Science

Alexander Heinlein, Mauro Perego, Sivasankaran Rajamanickam

FROSch Preconditioners for Land Ice Simulations of Greenland and Antarctica

Technical Report ID: CDS-2021-01

Available at <https://kups.uni-koeln.de/id/eprint/30668>

Submitted on January 25, 2021

FROSC PRECONDITIONERS FOR LAND ICE SIMULATIONS OF GREENLAND AND ANTARCTICA*

ALEXANDER HEINLEIN[†], MAURO PEREGO[‡], AND SIVASANKARAN RAJAMANICKAM[‡]

Abstract. Numerical simulations of Greenland and Antarctic ice sheets involve the solution of large-scale highly nonlinear systems of equations on complex shallow geometries. This work is concerned with the construction of Schwarz preconditioners for the solution of the associated tangent problems, which are challenging for solvers mainly because of the strong anisotropy of the meshes and wildly changing boundary conditions that can lead to poorly constrained problems on large portions of the domain. Here, two-level GDSW (Generalized Dryja–Smith–Widlund) type Schwarz preconditioners are applied to different land ice problems, i.e., a velocity problem, a temperature problem, as well as the coupling of the former two problems. We employ the MPI-parallel implementation of multi-level Schwarz preconditioners provided by the package FROSch (Fast and Robust Schwarz) from the Trilinos library. The strength of the proposed preconditioner is that it yields out-of-the-box scalable and robust preconditioners for the single physics problems.

To our knowledge, this is the first time two-level Schwarz preconditioners are applied to the ice sheet problem and a scalable preconditioner has been used for the coupled problem. The preconditioner for the coupled problem differs from previous monolithic GDSW preconditioners in the sense that decoupled extension operators are used to compute the values in the interior of the subdomains. Several approaches for improving the performance, such as reuse strategies and shared memory OpenMP parallelization, are explored as well.

In our numerical study we target both uniform meshes of varying resolution for the Antarctic ice sheet as well as non uniform meshes for the Greenland ice sheet are considered. We present several weak and strong scaling studies confirming the robustness of the approach and the parallel scalability of the FROSch implementation. Among the highlights of the numerical results are a weak scaling study for up to 32 K processor cores (8 K MPI-ranks and 4 OpenMP threads) and 566 M degrees of freedom for the velocity problem as well as a strong scaling study for up to 4 K processor cores (and MPI-ranks) and 68 M degrees of freedom for the coupled problem.

Key words. domain decomposition methods, monolithic Schwarz preconditioners, GDSW coarse spaces, multiphysics simulations, parallel computing

AMS subject classifications. 65F08, 65Y05, 65M55, 65N55

1. Introduction. Greenland and Antarctic ice sheets store most of the fresh water on earth and mass loss from these ice sheets significantly contributes to sea-level rise (see, e.g. [11]). In this work, we propose overlapping Schwarz domain decomposition preconditioners for efficiently solving the linear systems arising in the context of ice sheet modeling.

We first consider the solution of the ice sheet momentum equations for computing the ice velocity. This problem is at the core of ice sheet modeling and has been largely addressed in literature and several solvers have been considered [40, 6, 18, 35, 50, 19, 10, 9]. Most solvers from the literature rely on Newton-Krylov methods, using, e.g., the conjugate gradient (CG) [31] or the generalized minimal residual (GMRES) [44] method as the linear solver, and either one-level

*Submitted to the editors DATE.

[†]Institute for Applied Analysis and Numerical Simulation, University of Stuttgart, Germany. Department of Mathematics and Computer Science, University of Cologne (alexander.heinlein@uni-koeln.de). Center for Data and Simulation Science, University of Cologne (<http://www.cds.uni-koeln.de>).

[‡]Center for Computing Research, Scalable Algorithms Department, Sandia National Laboratories (mperego@sandia.gov, srajama@sandia.gov). Sandia National Laboratories is a multimission laboratory managed and operated by National Technology and Engineering Solutions of Sandia, LLC., a wholly owned subsidiary of Honeywell International, Inc., for the U.S. Department of Energy's National Nuclear Security Administration under contract DE-NA-0003525.

42 Schwarz preconditioners, hierarchical low-rank methods, or multigrid preconditioners
 43 to accelerate the convergence. In particular, the ones that have been demonstrated
 44 on problems with hundreds of millions of unknowns [6, 35, 50, 19, 10] use tailored
 45 multigrid preconditioners or hierarchical low-rank methods. Multigrid precondition-
 46 ers [6, 35, 50, 19] require careful design of the grid transfer operators for properly
 47 handling the anisotropy of the mesh and the basal boundary conditions that range
 48 from no-slip to free-slip. Hierarchical low-rank approaches have also been used for the
 49 velocity problem [10, 9]. Chen et al. [10] developed a parallel hierarchical low-rank
 50 preconditioner that is asymptotically scalable, but it has a large constant overhead
 51 and the trade-off between memory usage and solver convergence does not make it
 52 an ideal choice for the large problems considered here. The hierarchical low-rank
 53 approach that showed the most promise in terms of solver scalability is a sequential
 54 implementation limiting its usage to small problems [9].

55 In addition to the velocity problem, we also consider the problem of finding the
 56 temperature of an ice sheet using an enthalpy formulation ([1, 46, 32]) and the steady-
 57 state thermo-mechanical problem coupling the velocity and the temperature problems.
 58 The robust solution of this coupled problem is crucial for finding the initial thermo-
 59 mechanical state of the ice sheet under the assumption that the problem is almost
 60 at thermodynamic equilibrium. In fact, the initial state is estimated solving a PDE-
 61 constrained optimization problem where the loss function is the mismatch with ob-
 62 servations and the constraint is the coupled velocity-temperature problem considered
 63 here. To our knowledge, while there are works in the literature targeting the solution
 64 of unsteady versions of the coupled problem ([5, 39, 43]), none of them targets the
 65 steady thermo-mechanical problem at the ice sheet scale.

66 Both the velocity problem and the coupled velocity-temperature problem are
 67 characterized by strong nonlinearities and anisotropic meshes (due to the shallow
 68 nature of ice sheets). The coupled problem presents additional complexities due to the
 69 different nature of the velocity and temperature equations, the former being a purely
 70 diffusive elliptic problem, whereas the second is an advection dominated problem. In
 71 our experience, the naive use of multigrid methods leads to convergence failure for
 72 the coupled problem.

73 Our approach is to employ a preconditioning framework based on two-level Schwarz
 74 methods with GDSW (Generalized Dryja–Smith–Wildund) [12, 13, 22, 23] type coarse
 75 spaces. To our knowledge, scalable domain decomposition methods such as the GDSW
 76 preconditioner used in this work have not been shown to work on the ice sheet prob-
 77 lems. The main contributions of this work are:

- 78 • We demonstrate that two-level Schwarz preconditioners such as GDSW (Gen-
 79 eralized Dryja–Smith–Wildund) type preconditioners work out-of-the-box to
 80 solve two single physics problems (the velocity problem and the temperature
 81 problem) on land ice simulations.
- 82 • We introduce a scalable two-level preconditioner for the coupled problem that
 83 is tailored for the coupled problem by decoupling the extension operators to
 84 compute the values in the interior of the subdomains.
- 85 • We present results using an MPI-parallel implementation of multi-level Schwarz
 86 preconditioners provided by the package FROSch (Fast and Robust Schwarz)
 87 from the Trilinos software framework.
- 88 • Finally, we demonstrate the scalability of the approach with several weak
 89 and strong scaling studies confirming the robustness of the approach and
 90 the parallel scalability of the FROSch implementation. We conduct a weak
 91 scaling study for up to 32K processor cores and 566 M degrees of freedom for

92 the velocity problem as well as a strong scaling study for up to 4K processor
 93 cores and 68M degrees of freedom for the coupled problem. We compare
 94 against the multigrid method in [48, 50] for the velocity problem.

95 The remainder of the paper is organized as follows. Sections 2 and 3 introduces the ice
 96 sheet problems and the finite element discretization used in this study. We describe
 97 the Schwarz preconditioners, the reuse strategies for better performance and the way
 98 we tailor the preconditioner for the coupled problem in Section 4. Our software
 99 framework, which is based on Albany and FROSch, is briefly described in Section
 100 5. Finally, the scalability and the performance of the proposed preconditioners are
 101 shown in Section 6.

102 **2. Mathematical model.** At the scale of glaciers and ice sheets, ice can be
 103 modeled as a very viscous shear-thinning fluid with a rheology that depends on the
 104 ice temperature. Complex phenomena like the formation of crevasses and ice calving
 105 would require more complex damage mechanics models, however the fluid descrip-
 106 tion accounts for most of the large scale dynamics of ice sheets and it is adopted
 107 by all ice sheet computational models. The ice temperature depends on ice flow
 108 (velocity/deformation). Given the large characteristic time scale of the temperature
 109 evolution, it is reasonable to assume the temperature to be relatively constant over
 110 a few decades and solve the flow problem uncoupled from the temperature problem.
 111 However, when finding the initial state of an ice sheet (by solving an inverse problem)
 112 it is important to consider the coupled flow/temperature model, to find a self con-
 113 sistent initial thermo-mechanical state. In this case, we assume the ice temperature
 114 to be almost in steady-state. Therefore, in this paper, we consider a steady-state
 115 temperature solver. In this section, we first introduce separately the flow model and
 116 the temperature model and then the coupled model.

2.1. Flow model. We model the ice as a very viscous shear-thinning fluid with
 velocity \mathbf{u} and pressure p satisfying the Stokes equations:

$$\begin{cases} -\nabla \cdot \sigma(\mathbf{u}, p) &= \rho_i \mathbf{g}, \\ \nabla \cdot \mathbf{u} &= 0, \end{cases}$$

117 where \mathbf{g} is the gravity acceleration, ρ_i the ice density and σ the stress tensor. In what
 118 follows, we use the so called first-order (FO) or Blatter-Pattyn approximation of the
 119 Stokes equations derived using scaling arguments based on the fact that ice sheets are
 120 shallow. Following [42] and [47], we have

$$121 \quad (2.1) \quad \begin{cases} -\nabla \cdot (2\mu \dot{\epsilon}_1) &= -\rho_i g \partial_x s, \\ -\nabla \cdot (2\mu \dot{\epsilon}_2) &= -\rho_i g \partial_y s, \end{cases}$$

122 where x and y are the horizontal coordinate vectors in a Cartesian reference frame,
 123 $s(x, y)$ is the ice surface elevation, $g = |\mathbf{g}|$, and $\dot{\epsilon}_1$ and $\dot{\epsilon}_2$ are given by

$$124 \quad (2.2) \quad \dot{\epsilon}_1 = (2\dot{\epsilon}_{xx} + \dot{\epsilon}_{yy}, \dot{\epsilon}_{xy}, \dot{\epsilon}_{xz})^T \quad \text{and} \quad \dot{\epsilon}_2 = (\dot{\epsilon}_{xy}, \dot{\epsilon}_{xx} + 2\dot{\epsilon}_{yy}, \dot{\epsilon}_{yz})^T.$$

125 Denoting with u and v the horizontal components of the velocity \mathbf{u} , the stress com-
 126 ponents are defined as $\epsilon_{xx} = \partial_x u$, $\epsilon_{xy} = \frac{1}{2}(\partial_y u + \partial_x v)$, $\epsilon_{yy} = \partial_y v$, $\epsilon_{xz} = \frac{1}{2}\partial_z u$ and
 127 $\epsilon_{yz} = \frac{1}{2}\partial_z v$. The ice viscosity μ in Eq. (2.1) is given by

$$128 \quad (2.3) \quad \mu = \frac{1}{2}A(T)^{-\frac{1}{n}} \dot{\epsilon}_e^{\frac{1-n}{n}},$$

129 where $A(T) = \alpha_1 e^{\alpha_2 T}$ is a temperature-dependent rate factor (see [47] for the defi-
 130 nition of coefficients α_1 and α_2), $n = 3$ is the power-law exponent, and the effective
 131 strain rate, $\dot{\epsilon}$, is defined as

$$132 \quad (2.4) \quad \dot{\epsilon}_e \equiv \left(\dot{\epsilon}_{xx}^2 + \dot{\epsilon}_{yy}^2 + \dot{\epsilon}_{xx}\dot{\epsilon}_{yy} + \dot{\epsilon}_{xy}^2 + \dot{\epsilon}_{xz}^2 + \dot{\epsilon}_{yz}^2 \right)^{\frac{1}{2}},$$

133 where $\dot{\epsilon}_{ij}$ are the corresponding strain-rate components. Given that the atmospheric
 134 pressure is negligible compared to the pressure in the ice, we prescribe stress-free
 135 conditions at the the upper surface:

$$136 \quad (2.5) \quad \dot{\epsilon}_1 \cdot \mathbf{n} = \dot{\epsilon}_2 \cdot \mathbf{n} = 0,$$

137 where \mathbf{n} is the outward pointing normal vector at the ice sheet upper surface, $z =$
 138 $s(x, y)$. The lower surface can slide according to the following Robin-type boundary
 139 condition

$$140 \quad 2\mu_e \dot{\epsilon}_1 \cdot \mathbf{n} + \beta u = 0, \quad 2\mu_e \dot{\epsilon}_2 \cdot \mathbf{n} + \beta v = 0,$$

141 where β is a spatially variable friction coefficient and u and v are the horizontal
 142 components of the velocity \mathbf{u} . The field β is set to zero beneath floating ice. On
 143 lateral boundaries we prescribe the conditions

$$144 \quad (2.6) \quad 2\mu_e \dot{\epsilon}_1 \cdot \mathbf{n} = \frac{1}{2}gH(\rho_i - \rho_w r^2)n_1 \quad \text{and} \quad 2\mu_e \dot{\epsilon}_2 \cdot \mathbf{n} = \frac{1}{2}gH(\rho_i - \rho_w r^2)n_2,$$

145 where \mathbf{n} is the outward pointing normal vector to the lateral (i.e., parallel to the (x, y)
 146 plane), ρ_w is the density of ocean water, n_1 and n_2 are the x and y component of \mathbf{n} ,
 147 and r is the ratio of ice thickness that is submerged. On terrestrial ice margins $r = 0$,
 148 whereas on floating ice $r = \frac{\rho_i}{\rho_w}$. Additional details on the momentum balance solver
 149 can be found in [47].

2.2. Temperature model. As apparent from (2.3), the ice rheology depends
 on the ice temperature T . In order to model the ice sheet thermal state, we consider
 an enthalpy formulation similar to the one proposed by Aschwanded et al. in [1]. We
 assume that, for cold ice, the enthalpy h depends linearly on the temperature, whereas
 for temperate ice, the enthalpy grows linearly with the water content ϕ

$$h = \begin{cases} \rho_i c (T - T_0), & \text{for cold ice } (h \leq h_m), \\ h_m + \rho_w L \phi, & \text{for temperate ice.} \end{cases}$$

150 Here, the melting enthalpy h_m is defined as $h_m := \rho_w c (T_m - T_0)$ and T_0 is a uniform
 151 reference temperature.

152 The steady state enthalpy equation reads

$$153 \quad (2.7) \quad \nabla \cdot \mathbf{q}(h) + \mathbf{u} \cdot \nabla h = 4\mu_e \dot{\epsilon}_e^2.$$

Here, $\mathbf{q}(h)$ is the enthalpy flux, given by

$$\mathbf{q}(h) = \begin{cases} \frac{k}{\rho_i c_i} \nabla h, & \text{for cold ice } (h \leq h_m), \\ \frac{k}{\rho_i c_i} \nabla h_m + \rho_w L \mathbf{j}(h), & \text{for temperate ice,} \end{cases}$$

$\mathbf{u} \cdot \nabla h$ is the drift term, and $4\mu_e \dot{\epsilon}_e^2$ is the heat associated to ice deformation. The water
 flux term

$$\mathbf{j}(h) := \frac{1}{\eta_w} (\rho_w - \rho_i) k_0 \phi^\gamma \mathbf{g}$$

has been introduced by Schoof and Hewitt ([46, 32]), and it describes the percolation of water driven by gravity. The parameter c_i is the heat capacity of ice, k its thermal conductivity, and L is the latent heat of fusion. At the upper surface, the enthalpy is set to $h = \rho_i c(T_s - T_0)$, where T_s is the temperature of the air at the ice upper surface. At the bed, the ice is either in contact with a dry bed or with a film of water at the melting point temperature and, in first approximation, satisfies the Stefan condition:

$$m = G + \beta\sqrt{u^2 + v^2} - k\nabla T \cdot \mathbf{n} \quad \text{and} \quad m(T - T_m) = 0 \quad \text{and} \quad T_m \leq 0.$$

154 Here, m is the melting rate. Ice at the bed is melting when $m > 0$ and refreezing
 155 when $m < 0$. Moreover, G is the geothermal heat flux (positive if entering the ice
 156 domain), $\beta\sqrt{u^2 + v^2}$ is the frictional heat, and $-k\nabla T \cdot \mathbf{n}$ is the temperature heat flux
 157 exiting the domain as \mathbf{n} is the outer normal to the ice domain. Depending on whether
 158 the ice is cold at the bed, melting or refreezing, the Stefan condition translates into
 159 natural or essential boundary conditions for the enthalpy equation. Further details
 160 on the enthalpy formulation and its discretization are provided in [41].

161 **2.3. Coupled model.** The ice velocity depends on the temperature through
 162 (2.4), and the enthalpy depends on the velocity field through the drift term $\mathbf{u} \cdot \nabla h$
 163 and the fractional heat term at the ice sheet lower surface. The first order problem
 164 (2.1) only provides the horizontal velocities u and v , but we also need the vertical
 165 velocity w to solve the enthalpy equations. The vertical velocity w is computed using
 166 the incompressibility condition

$$167 \quad (2.8) \quad \partial_x u + \partial_y v + \partial_z w = 0,$$

with the Dirichlet boundary condition at the ice lower surface

$$\mathbf{u} \cdot \mathbf{n} = \frac{m}{L(\rho_i - \rho_w \phi)}.$$

168 The coupled problem is formed by problems (2.1), (2.8) and (2.7) and their respective
 169 boundary conditions. For further details, see [41]. Figure 1 shows the ice velocity and
 170 temperature computed solving the coupled thermo-mechanical model. For details
 171 about the problem setting and the Greenland data set, see [41].

172 **3. Finite element discretization.** The ice sheet mesh is generated by extrud-
 173 ing in the vertical direction a two dimensional unstructured mesh of the ice sheet
 174 horizontal extension ([47]) and it is constituted of layers of prisms. The problems
 175 described in section 2 are discretized with continuous piece-wise bi-linear (for trian-
 176 gular prisms) or tri-linear (for hexahedra) finite elements using a standard Galerkin
 177 formulation, for each component of the velocity and for the enthalpy. We use up-
 178 wind stabilization for the enthalpy equation. The nonlinear discrete problems can be
 179 written in the residual form

$$180 \quad (3.1) \quad F(x) = 0,$$

182 where x is the problem unknown (velocity, enthalpy, or both, depending on the prob-
 183 lem). The nonlinear problems are then solved using a Newton-Krylov approach. More
 184 precisely, we linearize the problem using Newton's method, and solve the resulting
 185 linear tangent problems

$$186 \quad (3.2) \quad DF(x^{(k)})\Delta x^{(k)} = -F(x^{(k)})$$

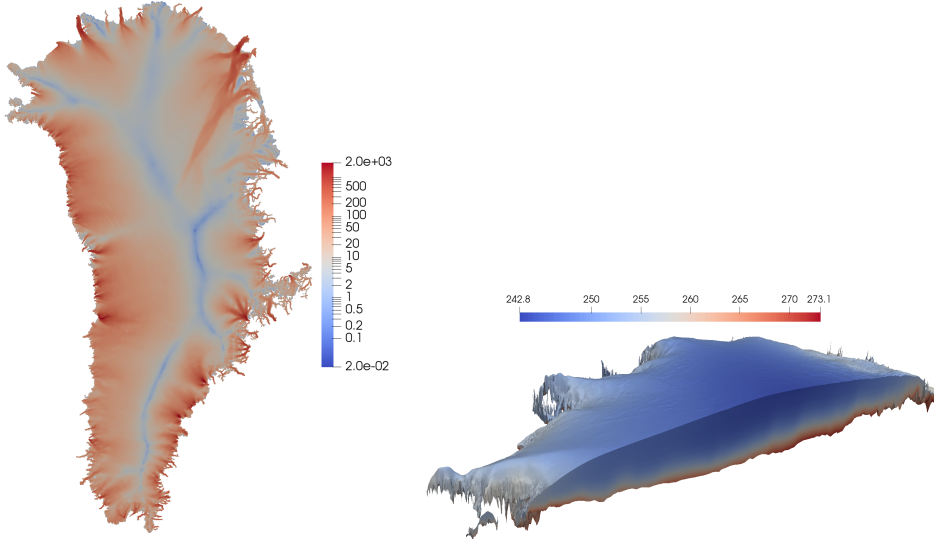


FIG. 1. *Solution of a Greenland ice sheet simulation. Left: ice surface speed in [m/yr], Right: ice temperature in [K] over a vertical section of the ice sheet.*

188 using a Krylov subspace method. The Jacobian DF is computed through automatic
 189 differentiation. At each nonlinear iteration, we solve a problem of the form

$$190 \quad (3.3) \quad Ax = r,$$

192 where A is the tangent matrix $DF(x^{(k)})$, and r is the residual vector $-F(x^{(k)})$. Using
 193 a block matrix notation, the tangent problem of the velocity problem can be written
 194 as

$$195 \quad (3.4) \quad \begin{bmatrix} A_{uu} & A_{uv} \\ A_{vu} & A_{vv} \end{bmatrix} \begin{bmatrix} x_u \\ x_v \end{bmatrix} = \begin{bmatrix} r_u \\ r_v \end{bmatrix}$$

197 where the tangent matrix is symmetric positive definite. When considering also the
 198 vertical velocity w , the tangent problem becomes

$$199 \quad (3.5) \quad \underbrace{\begin{bmatrix} A_{uu} & A_{uv} \\ A_{vu} & A_{vv} \\ A_{wu} & A_{wv} & A_{ww} \end{bmatrix}}_{=:A_u} \underbrace{\begin{bmatrix} x_u \\ x_v \\ x_w \end{bmatrix}}_{=:x_u} = \underbrace{\begin{bmatrix} r_u \\ r_v \\ r_w \end{bmatrix}}_{=:r_u}$$

201 Note that the matrix is lower block-triangular because in the FO approximation, the
 202 horizontal velocities are independent of the vertical velocity. Similarly, the tempera-
 203 ture equation reads

$$204 \quad (3.6) \quad A_T x_T = r_T.$$

206 The coupled problem is a multiphysics problem coupling the velocity and the
 207 temperature problem. Hence, the tangent system can be written as

$$208 \quad (3.7) \quad \begin{bmatrix} A_u & C_{uT} \\ C_{Tu} & A_T \end{bmatrix} \begin{bmatrix} x_u \\ x_T \end{bmatrix} = \begin{bmatrix} \tilde{r}_u \\ \tilde{r}_T \end{bmatrix},$$

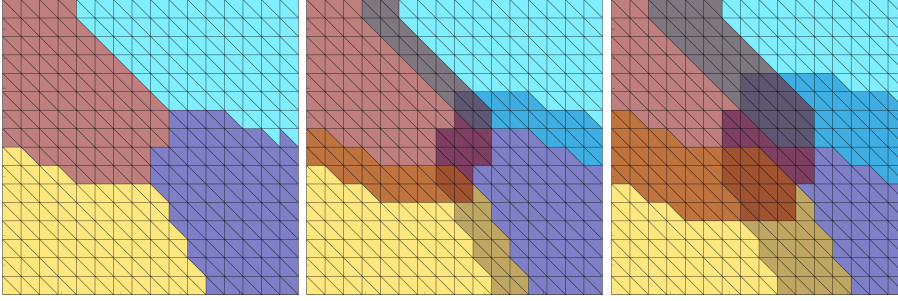


FIG. 2. Extending two-dimensional nonoverlapping subdomains (left) by layers of elements to obtain overlapping domain decompositions with an overlap of $\delta = 1h$ (middle) and $\delta = 2h$ (right).

210 where the blocks A_u and A_T and solution vectors x_u x_T are the same as in the single
 211 physics problems; cf. (3.5) and (3.6). The residual vectors \tilde{r}_u and \tilde{r}_T differ from the
 212 single physics residuals r_u and r_T due to the coupling of velocity and temperature,
 213 which also results in the nonzero coupling blocks C_{uT} and C_{Tu} in the
 214 tangent matrix.

215 **4. Preconditioners.** In order to solve the tangent problems (3.2) in our Newton
 216 iteration, we apply the generalized minimal residual (GMRES) method [44] and speed
 217 up the convergence using generalized Dryja–Smith–Widlund (GDSW) type domain
 218 decomposition preconditioners. In particular, we will use classical GDSW and reduced
 219 dimension GDSW (RGDSW) preconditioners, as described in subsection 4.1, as well
 220 as corresponding monolithic preconditioners, as introduced in subsection 4.3. In order
 221 to improve the performance of the first level of the Schwarz preconditioners, we will
 222 always apply scaled prolongation operators; cf. subsection 4.2. As we will describe
 223 in subsection 4.4, domain decomposition preconditioners and, in particular, GDSW
 224 type preconditioners are well-suited for the solution of land ice problems because
 225 of the specific structure of the meshes. In order to improve the efficiency of the
 226 preconditioners in our Newton-Krylov algorithm, we will also apply strategies to reuse,
 227 in later Newton iterations, certain components of the preconditioners set up in the
 228 first Newton iteration; see subsection 4.5.

229 For the sake of clarity, we will restrict ourselves to the case of uniform meshes
 230 with characteristic element size h for the description of the preconditioners. However,
 231 the methods can also be applied to non-uniform meshes as the ones for Greenland;
 232 see Figure 4.

233 **4.1. GDSW type preconditioners.** Let us consider the general linear system

$$234 \quad (4.1) \quad Ax = b$$

236 arising from a finite element discretization of an elliptic boundary value problem on
 237 Ω . Our aim is then to apply the preconditioners to the tangent problems (3.3) of the
 238 model problems described in section 2.

239 The GDSW preconditioner was originally introduced by Dohrmann, Klawonn,
 240 and Widlund in [13, 12] for elliptic problems. It is a two-level Schwarz preconditioner
 241 with energy minimizing coarse space and exact solvers. To describe the construction
 242 of the GDSW preconditioner, let Ω be partitioned into N nonoverlapping subdomains
 243 $\Omega_1, \dots, \Omega_N$ with characteristic size H . We extend these subdomains by adding k
 244 layers of finite elements resulting in overlapping subdomains $\Omega'_1, \dots, \Omega'_N$ with an overlap

245 $\delta = kh$; cf. Figure 2 for a two-dimensional example. In general, two-level Schwarz
 246 preconditioners for (4.1) with exact solvers are of the form

$$247 \quad (4.2) \quad M_{OS-2} = \underbrace{\Phi A_0^{-1} \Phi^T}_{\text{coarse level}} + \underbrace{\sum_{i=1}^N R_i^T A_i^{-1} R_i}_{\text{first level}}.$$

248
 249 Here, $A_0 = \Phi^T A \Phi$ is the coarse matrix corresponding to a Galerkin projection onto
 250 the coarse space, which is spanned by the columns of matrix Φ . The local matrices A_i
 251 are submatrices of A corresponding to the overlapping subdomains $\Omega'_1, \dots, \Omega'_N$. They
 252 can be written as $A_i = R_i A R_i^T$, where $R_i : V^h \rightarrow V_i^h$ is the restriction operator from
 253 the global finite element space V^h to the local finite element space V_i^h on Ω'_i ; the R_i^T
 254 is the corresponding prolongation.

255 We first present the framework enabling the construction of energy-minimizing
 256 coarse spaces for elliptic problems based on a partition of unity on the interface

$$257 \quad (4.3) \quad \Gamma = \{x \in (\bar{\Omega}_i \cap \bar{\Omega}_j) \setminus \partial\Omega_D \mid i \neq j, 1 \leq i, j \leq N\}$$

258
 259 of the nonoverlapping domain decomposition, where $\partial\Omega_D$ is the Dirichlet boundary.
 260 This will allow us to construct classical GDSW coarse spaces [13, 12] and reduced
 261 dimension GDSW coarse spaces [16] as used in our simulations. Note that other
 262 types of coarse spaces can be constructed using this framework as well, e.g., coarse
 263 spaces based on the MsFEM (Multiscale Finite Element Method) [34]; see also [7].
 264 However, in our experiments, we restrict ourselves to the use of GDSW type coarse
 265 spaces.

266 Let us first decompose Γ into connected components $\Gamma_1, \dots, \Gamma_M$. This decom-
 267 position of Γ may be overlapping or nonoverlapping. Furthermore, let R_{Γ_i} be the
 268 restriction from all interface degrees of freedom to the degrees of freedom of the in-
 269 terface component Γ_i . In order to account for overlapping decompositions of the
 270 interface, we introduce diagonal scaling matrices D_{Γ_i} , such that

$$271 \quad (4.4) \quad \sum_{i=1}^M R_{\Gamma_i}^T D_{\Gamma_i} R_{\Gamma_i} = I_\Gamma,$$

272
 273 where I_Γ is the identity matrix on Γ . This means that the scaling matrices correspond
 274 to a partition of unity on the interface Γ .

275 Using the scaling matrices D_{Γ_i} , we can now build a space which can represent the
 276 restriction of the null space of our problem to the interface. Therefore, let the columns
 277 of the matrix Z form a basis of the null space of the operator \hat{A} , which is the global
 278 matrix corresponding to A but with homogeneous Neumann boundary conditions on
 279 the full boundary, and let the Z_Γ be restriction of Z to the interface Γ . Because of
 280 (4.4), we have

$$281 \quad \sum_{i=1}^M R_{\Gamma_i}^T D_{\Gamma_i} R_{\Gamma_i} Z_\Gamma = Z_\Gamma.$$

282
 283 Now, for each Γ_i , we construct a matrix Φ_{Γ_i} such that its columns are a basis of
 284 the space spanned by the columns of $D_{\Gamma_i} R_{\Gamma_i} Z_\Gamma$. Then, the interface values of our
 285 coarse space are given by the matrix

$$286 \quad (4.5) \quad \Phi_\Gamma = [R_{\Gamma_1}^T \Phi_{\Gamma_1} \quad \dots \quad R_{\Gamma_M}^T \Phi_{\Gamma_M}].$$

287 Based on these interface values, the coarse basis functions are finally computed
 288 as energy-minimizing extensions to the interior of the nonoverlapping subdomains.
 289 Therefore, we partition all degrees of freedom into interface (Γ) and interior (I) degrees
 290 of freedom. Then, the system matrix can be written as

$$291 \quad A = \begin{bmatrix} A_{II} & A_{I\Gamma} \\ A_{\Gamma I} & A_{\Gamma\Gamma} \end{bmatrix}$$

293 and the energy-minimizing extensions are computed as $\Phi_I = -A_{II}^{-1}A_{I\Gamma}\Phi_\Gamma$, resulting
 294 in the coarse basis

$$295 \quad (4.6) \quad \Phi = \begin{bmatrix} \Phi_I \\ \Phi_\Gamma \end{bmatrix} = \begin{bmatrix} -A_{II}^{-1}A_{I\Gamma}\Phi_\Gamma \\ \Phi_\Gamma \end{bmatrix}.$$

296 As mentioned earlier, this construction allows for a whole family of coarse spaces,
 297 depending on decomposition of the interface into components Γ_i and the choice of
 298 scaling matrices D_{Γ_i} .

299 *GDSW coarse spaces.* We obtain the interface components of the GDSW coarse
 300 space $\Gamma_i^{(\text{GDSW})}$ by decomposing the interface Γ into the largest connected components
 301 γ belonging to the same sets of subdomains \mathcal{N}_γ , i.e., into vertices, edges, and faces;
 302 cf., e.g., [38]. More precisely,

$$303 \quad \mathcal{N}_\gamma := \{i : x \in \overline{\Omega}_i \ \forall x \in \gamma\}.$$

304 Because these components are disjoint by construction, the scaling matrices $D_{\Gamma_i^{(\text{GDSW})}}$
 305 have to be chosen as identity matrices $I_{\Gamma_i^{(\text{GDSW})}}$ in order to satisfy (4.4). Using this
 306 choice, we obtain the classical GDSW coarse space as introduced by Dohrmann, Klau-
 307 wonn, and Widlund in [13, 12]. If the boundaries of the subdomains are uniformly
 308 Lipschitz, the condition number estimate for the resulting two-level GDSW precondi-
 309 tioner,

$$310 \quad (4.7) \quad \kappa(M_{\text{GDSW}}^{-1}A) \leq C \left(1 + \frac{H}{\delta}\right) \left(1 + \log\left(\frac{H}{h}\right)\right),$$

312 holds for scalar elliptic and compressible linear elasticity model problems; the constant
 313 C is then independent of the geometrical parameters H , h , and δ . For the general case
 314 of $\Omega \subset \mathbb{R}^2$ being decomposed into John domains, we can obtain a condition number
 315 estimate with a second power logarithmic term, i.e., with $(1 + \log(\frac{H}{h}))^2$ instead of
 316 $(1 + \log(\frac{H}{h}))$; cf. [12, 13]. Please also refer to [14, 15] for other variants with linear
 317 logarithmic term.

318 *RGDSW coarse spaces.* Another choice of the Γ_i leads to reduced dimension
 319 GDSW (RGDSW) coarse spaces; cf. [16]. In order to construct the interface com-
 320 ponents $\Gamma_i^{(\text{RGDSW})}$, we first define a hierarchy of the previously defined $\Gamma_i^{(\text{GDSW})}$. In
 321 particular, we call an interface component γ *ancestor* of another interface compo-
 322 nent γ' if $\mathcal{N}_{\gamma'} \subset \mathcal{N}_\gamma$; conversely, we call γ *offspring* of γ' if $\mathcal{N}_{\gamma'} \supset \mathcal{N}_\gamma$. Now, let
 323 $\{\hat{\Gamma}_i^{(\text{GDSW})}\}_{i=1, \dots, M^{(\text{RGDSW})}}$ be the set of all GDSW interface components which have
 324 no ancestors; we call these *coarse components*. Now, we define the RGDSW interface
 325 components as

$$326 \quad (4.8) \quad \Gamma_i^{(\text{RGDSW})} := \bigcup_{\mathcal{N}_\gamma \subset \mathcal{N}_{\hat{\Gamma}_i^{(\text{GDSW})}}} \gamma, \quad \forall i = 1, \dots, M^{(\text{RGDSW})}.$$

327

328 The $\Gamma_i^{(\text{RGDSW})}$ may overlap in nodes which do not belong to the coarse components.
 329 Hence, we have to introduce scaling operators $D_{\Gamma_i^{(\text{RGDSW})}} \neq I_{\Gamma_i^{(\text{RGDSW})}}$ to obtain a
 330 partition of unity on the interface; cf. (4.4). Different scaling operators D_{Γ_i} lead to
 331 different variants of RGDSW coarse spaces, e.g., Options 1, 2.1, and 2.2, introduced
 332 in [16] and another variant introduced in [25]. Here, we will only consider the algebraic
 333 variant, Option 1, where an inverse multiplicity scaling

$$334 \quad D_{\Gamma_i^{(\text{RGDSW})}} = R_{\Gamma_i^{(\text{RGDSW})}} \left(\sum_{j=1}^{M(\text{RGDSW})} R_{\Gamma_j^{(\text{RGDSW})}}^T R_{\Gamma_j^{(\text{RGDSW})}} \right)^{-1} R_{\Gamma_i^{(\text{RGDSW})}}^T.$$

335

336 is employed. Under the condition that all subdomains are Lipschitz domains, we then
 337 obtain the same condition number estimate as previously for GDSW coarse spaces

$$338 \quad (4.9) \quad \kappa(M_{\text{RGDSW}}^{-1}A) \leq C \left(1 + \frac{H}{\delta} \right) \left(1 + \log \left(\frac{H}{h} \right) \right);$$

339

340 for scalar elliptic and compressible linear elasticity model problems; cf. [16].

341 The only missing ingredient to construct the GDSW and RGDSW coarse spaces
 342 is the respective the null space Z of the global Neumann matrix corresponding to A .
 343 For the velocity and the temperature problem, the preconditioners can be directly
 344 constructed and applied using the corresponding null spaces spanned by

$$345 \quad r_{u,1} := \begin{bmatrix} 1 \\ 0 \end{bmatrix}, r_{u,2} := \begin{bmatrix} 0 \\ 1 \end{bmatrix} \quad \text{and} \quad r_{u,3} := \begin{bmatrix} y \\ -x \end{bmatrix}$$

346 or

$$347 \quad r_T := [1],$$

348 respectively, on each finite element node. Here, $r_{u,1}$ and $r_{u,2}$ correspond to the transla-
 349 tions and $r_{u,3}$ to the linearized rotation building the null space of the velocity problem.
 350 The r_T is the constant null space element of the temperature problem.

351 *Remark 4.1.* Sometimes it may be beneficial to only consider a subspace \hat{Z} of the
 352 full space Z . This results in a smaller coarse space, at the cost of slower convergence of
 353 the linear solver. In particular, in theory, numerical scalability is not provided in this
 354 case. However, since the coarse solve is typically a parallel scaling bottleneck, it may
 355 still be faster to neglect a part of the coarse space for a large number of subdomains.
 356 In our numerical results, we will actually observe that neglecting rotational rigid body
 357 modes improves the parallel performance of our solver; see also [28, 24] for similar
 358 experiments for elasticity problems.

359 Note that, if rotations are neglected, the GDSW and RGDSW coarse spaces
 360 are actually constructed in an algebraic way because the translational coarse basis
 361 functions can be computed without geometric information; see also the discussion
 362 in [24].

363 For the coupled problem described in subsection 2.3, we will describe an mono-
 364 lithic preconditioner in subsection 4.3, where we use the same construction but with
 365 decoupled extensions operators. Before that, however, we will describe the scaled
 366 prolongation operators used in the first level in our numerical experiments.

367 **4.2. Scaled prolongation operators.** As first shown in [8], the convergence
 368 of additive Schwarz preconditioners can often be improved using restricted or scaled
 369 variants of the prolongation operators R_i^T in (4.2); see also [17, 23]. For the sake of
 370 brevity, we will not compare the performance of the standard, the restricted, and the
 371 scaled variants for the different model problems considered in this paper. We only
 372 show results using the scaled variant because it performed best in preliminary tests.

373 We construct the scaled prolongation operator \tilde{R}_i^T such that $\sum_{i=1}^N \tilde{R}_i^T R_i = I$:

$$374 \quad \tilde{R}_i^T := \left(\sum_{j=1}^N R_j^T R_j \right)^{-1} R_i^T.$$

376 Note that the matrix $\sum_{i=1}^N R_i^T R_i$ is just a diagonal scaling matrix, and its inverse
 377 can therefore be specified directly. The two-level Schwarz preconditioner with scaled
 378 prolongations then reads

$$379 \quad M_{OS-2} = \Phi A_0^{-1} \Phi^T + \sum_{i=1}^N \tilde{R}_i^T A_i^{-1} R_i.$$

382 **4.3. Monolithic preconditioning the coupled problem.** For the coupled
 383 problem, A is structured as follows

$$384 \quad (4.10) \quad A = \begin{bmatrix} A_{uu} & A_{uT} \\ A_{Tu} & A_{TT} \end{bmatrix},$$

386 where the off-diagonal blocks formally account for the coupling of the different vari-
 387 ables; cf. section 3. We will construct monolithic two-level Schwarz preconditioners as
 388 introduced in [36, 37] and extended to monothic GDSW preconditioners in [22, 23].
 389 Formally, the monolithic preconditioners for the coupled problem can again be written
 390 as

$$391 \quad (4.11) \quad M_{OS-2} = \Phi A_0^{-1} \Phi^T + \sum_{i=1}^N \tilde{R}_i^T A_i^{-1} R_i.$$

393 However, all matrices are now 2×2 block-matrices. In particular, the monolithic
 394 restriction and prolongation matrices are of the form

$$395 \quad R_i = \begin{bmatrix} R_{i,u} & 0 \\ 0 & R_{i,T} \end{bmatrix} \quad \text{and} \quad \tilde{R}_i = \begin{bmatrix} \tilde{R}_{i,u} & 0 \\ 0 & \tilde{R}_{i,T} \end{bmatrix},$$

397 where $R_{i,u}$ and $R_{i,T}$ are the restriction operators to the overlapping subdomain Ω'_i on
 398 the velocity and temperature degrees of freedom, and $\tilde{R}_{i,u}$ and $\tilde{R}_{i,T}$ are the respective
 399 prolongations operators.

400 The coarse space can be constructed in a similar way as in the single physics
 401 case. In particular, the interface components Γ_i and the scaling matrices D_{Γ_i} are
 402 constructed in the same way, and the null space Z of the multi physics problem
 403 is composed of the null spaces of the individual single physics problems. However,
 404 as we will observe in the numerical results, it is necessary to remove the coupling
 405 blocks between the velocity and the temperature problem before computing the ex-
 406 tensions (4.6). Hence, instead of A , the matrix

$$407 \quad (4.12) \quad \tilde{A} = \begin{bmatrix} A_{uu} & 0 \\ 0 & A_{TT} \end{bmatrix}$$

409 is used in the computation of the harmonic extensions, i.e., $\Phi_I = -\tilde{A}_{II}^{-1}\tilde{A}_{I\Gamma}\Phi_\Gamma$. This
 410 can be viewed as applying a block Jacobi preconditioner with two blocks corresponding
 411 to the single physics problems instead of solving the systems corresponding to A_{II}^{-1}
 412 monolithically. Consequently, the coarse basis functions corresponding to the velocity
 413 and the temperature problem can be computed independently. Then, the matrix Φ
 414 is of the form

$$415 \quad (4.13) \quad \Phi = \begin{bmatrix} \Phi_{u,u_0} & 0 \\ 0 & \Phi_{T,T_0} \end{bmatrix},$$

417 where the row indices u and T indicate the finite element functions of the original
 418 problem, and column indices u_0 and T_0 correspond to the basis functions of the coarse
 419 space. A similar decoupling approach for the coarse basis functions was performed
 420 in [22, 23] for a monolithic preconditioner for fluid problems. However, it was neces-
 421 sary to first compute the fully coupled extensions (4.6) and to drop the off diagonal
 422 blocks in the matrix Φ afterwards. This was due to the fact that the system matrix
 423 was of the form $\begin{bmatrix} A & B^T \\ B & 0 \end{bmatrix}$, such that the decoupled matrix would become singular.

424 Here, the decoupled matrix (4.12) remains invertible since the individual blocks corre-
 425 spond to the single physics velocity and temperature problems. Therefore, our coarse
 426 basis matrix is also of the same structure for Lagrangian coarse spaces in [36, 37].

427 It is important to note that, even though the coarse basis functions do not contain
 428 any coupling blocks, the coarse problem is still a coupled problem with a coarse matrix
 429 of the form

$$430 \quad A_0 = \begin{bmatrix} \Phi_{u,u_0} & 0 \\ 0 & \Phi_{T,T_0} \end{bmatrix}^T \begin{bmatrix} A_{uu} & A_{uT} \\ A_{Tu} & A_{TT} \end{bmatrix} \begin{bmatrix} \Phi_{u,u_0} & 0 \\ 0 & \Phi_{T,T_0} \end{bmatrix}$$

$$431 \quad = \begin{bmatrix} \Phi_{u,u_0}^T A_{uu} \Phi_{u,u_0} & \Phi_{u,u_0}^T A_{uT} \Phi_{T,T_0} \\ \Phi_{T,T_0}^T A_{Tu} \Phi_{u,u_0} & \Phi_{T,T_0}^T A_{TT} \Phi_{T,T_0} \end{bmatrix}.$$

433 Because we use equal order discretizations for the velocity and temperature vari-
 434 ables in the coupled problem, we can formally apply a node wise ordering to our
 435 degrees of freedom. Then, the monolithic preconditioner can be constructed exactly
 436 as in the elliptic case (see section 4), however, using the previously described decou-
 437 pled matrix (4.12) to compute the extension.

438 We then obtain all three velocity degrees of freedom and one temperature degree
 439 of freedom for each finite element node. Therefore, the full null space is spanned by
 440 the null space corresponding to the three velocity degrees of freedom

$$441 \quad r_{u,1} := \begin{bmatrix} 1 \\ 0 \\ 0 \\ 0 \end{bmatrix}, \quad r_{u,2} := \begin{bmatrix} 0 \\ 1 \\ 0 \\ 0 \end{bmatrix}, \quad r_{u,3} := \begin{bmatrix} 0 \\ 0 \\ 1 \\ 0 \end{bmatrix}, \quad \text{and } r_{u,4} := \begin{bmatrix} y \\ -x \\ 0 \\ 0 \end{bmatrix}$$

442 as well as the null space on the temperature degree of freedom

$$443 \quad r_T := \begin{bmatrix} 0 \\ 0 \\ 0 \\ 1 \end{bmatrix}.$$

444 Here, $r_{u,4}$ corresponds to a linearized rotation, which will be neglected in some of our
 445 numerical experiments to reduce the computing time on the coarse level.

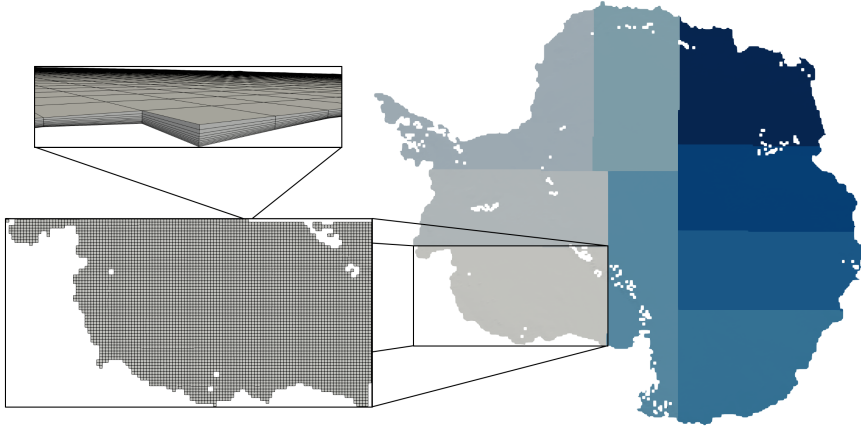


FIG. 3. Uniform hexahedral mesh for the Antarctica ice sheet with a horizontal resolution of 16 km decomposed into nine subdomains. The domain decomposition is performed on the two-dimensional top surface mesh, and the subdomains are extruded in vertical direction to obtain three-dimensional subdomains with 10 layers height.

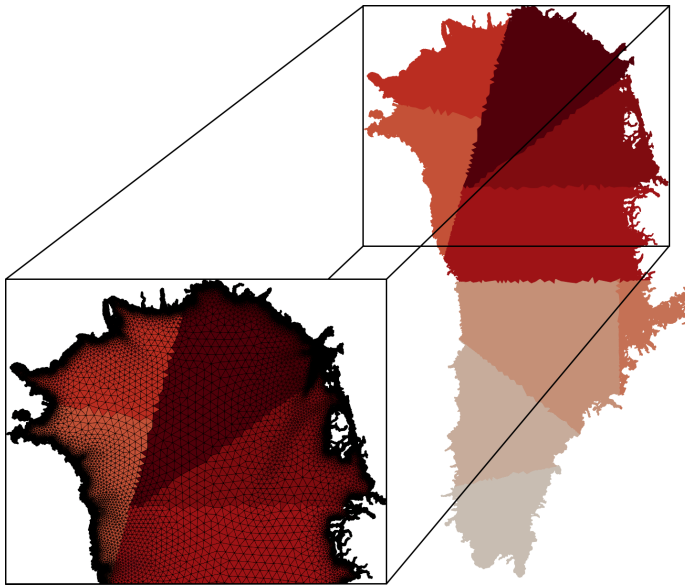


FIG. 4. Non-uniform triangulation of the top surface mesh for the Greenland ice sheet with a horizontal resolution of 3 km to 30 km decomposed into nine subdomains. The three-dimensional mesh is then obtained by extrusion in vertical direction.

446 **4.4. Remarks on domain decomposition methods for land ice problems.**
 447 The geometries for the ice sheets in Antarctica and Greenland are visualized in [Fig-](#)
 448 [ures 3](#) and [4](#). Generally, the horizontal extensions of the ice sheets are in the order of
 449 hundreds or thousands of kilometers, whereas their thickness is at maximum only a
 450 few kilometers. Therefore, the geometries and the corresponding meshes used in our
 451 simulations are clearly anisotropic; cf. [section 3](#) for a description of the mesh gener-
 452 ation procedure and [Figure 3](#) for a visualization of a exemplary mesh of Antarctica

reuse strategy	short description
NR (<i>no reuse</i>)	Set up the preconditioner from scratch in each nonlinear iteration.
IS (<i>index sets</i>)	Reuse the index sets for the overlapping subdomains and the interface components
SF1 (<i>symb. fact. lvl 1</i>)	Reuse the symbolic factorization of A_i .
SF2 (<i>symb. fact. lvl 2</i>)	Reuse the symbolic factorization of A_0 .
CB (<i>coarse basis</i>)	Reuse the coarse basis Φ .
CM (<i>coarse matrix</i>)	Reuse the coarse matrix A_0 .

TABLE 1

Reuse strategies for monolithic GDSW preconditioners (4.2) for nonlinear model problems.

453 with a horizontal mesh resolution of 16 km and 10 layers of elements in z direction.

454 Due to this specific structure of the meshes, we perform the domain decomposition
 455 into nonoverlapping subdomains as follows: First, we decompose the two-dimensional
 456 mesh of the top surface. We extrude the two-dimensional subdomains in z direction
 457 next resulting in a domain decomposition of the whole three-dimensional domain.
 458 Hence, the domain decomposition is essentially a two-dimensional domain decompo-
 459 sition, and the partition of the domain decomposition interface Γ into the components
 460 $\Gamma_i^{(\text{GDSW})}$ only yields edges and faces but no vertices. However, as can be seen in **Fig-**
 461 **ures 3** and **4**, the subdomain geometries can be very irregular due to the complex
 462 shape of the boundary of the ice sheets. Hence, the domain decomposition is not well
 463 suited for the use of classical Lagrangian coarse spaces, which would require the con-
 464 struction of a coarse triangulation of the geometry. However, this is not required for
 465 GDSW type coarse spaces which can be constructed without an additional coarse tri-
 466 angulation. Hence they can easily be constructed for the considered land ice problems.
 467

468 **4.5. Reuse strategies for nonlinear problems.** The model problems in **sec-**
 469 **tion 2** are highly nonlinear; as can be seen in **section 6**, the coupled problem requires
 470 a particularly high number of nonlinear iterations. Therefore, we will investigate sev-
 471 eral strategies to reuse information from the first iteration in later Newton iterations,
 472 such that the total time to solution can be improved. Note that other approaches
 473 where the information is updated in certain multiple Newton iterations, e.g. in every
 474 n th iteration, are also possible but out of the scope of this paper.

475 The different reuse strategies, which are listed in **Table 1**, are used in different
 476 numerical experiments in **section 6**. Since neither the topology nor the domain decom-
 477 position of our problem changes during the nonlinear iteration, it is a safe assumption
 478 that the index sets of the overlapping subdomains and the interface components stay
 479 the same. This saves mostly communication, which dominates the time for identify-
 480 ing the index sets; see **section 5**. If the sparsity pattern of the system matrix is also
 481 constant during the nonlinear iteration, the symbolic factorizations for A_i and A_0 can
 482 be easily reused as well.

483 In GDSW type preconditioners, the coarse basis functions Φ change with the
 484 tangent matrix, which is used to compute the extensions (4.6) in each nonlinear
 485 iteration. However, in practice, the coarse basis computed with the tangent matrix
 486 in the first Newton iteration can also be used in later iterations. In some cases, the
 487 complete coarse matrix A_0 and its factorization can even be reused.

488 **5. Software framework.** The land ice problems are implemented in Albany
 489 Land Ice (formerly referred to as Albany FELIX) [47, 45], a C++ finite element library
 490 that relies on the Trilinos packages [49] for MPI+X parallelism (Tpetra, Kokkos), lin-
 491 ear (Belos/AztecOO) and nonlinear (NOX) solvers, preconditioners (Ifpack2, Muelu,
 492 ShyLU, FROSch [20, 28, 27, 26]), discretization tools (STK, Intrepid2, Phalanx) and
 493 automatic differentiation (Sacado). Albany Land Ice is part of the land ice code MALI
 494 [33].

495 The GDSW type preconditioners described in section 4 are implemented in the
 496 FROSch framework [27, 26], which is part of Trilinos [49]. FROSch can use both
 497 distributed-memory parallelism using the Tpetra package of Trilinos and shared-
 498 memory parallelism while using the direct solvers interfaced through Amesos2 package
 499 of Trilinos [2]. With respect to shared-memory parallelism, in this paper, we restrict
 500 ourselves to using CPU threads. Specifically, we use the Pardiso solver provided with
 501 the Intel MKL software, which can also make use of shared-memory parallelism using
 502 OpenMP threads. FROSch is called from Albany Land Ice using the unified Trilino-
 503 nos solver interface Stratimikos and directly uses the Tpetra matrices and vectors
 504 which have been assembled in. Moreover, FROSch makes use of the index set of the
 505 nonoverlapping domain decomposition and the null space basis provided by Albany
 506 Land Ice in form of Tpetra map and multivector objects; cf. the discussion in [21].

507 **6. Numerical results.** In this section, we will present numerical results for the
 508 flow (subsection 2.1), temperature (subsection 2.2), and coupled (subsection 2.3) prob-
 509 lems. For the flow problem, we will use the uniform meshes for Antarctica, whereas we
 510 will use the non-uniform Greenland meshes for the two other model problems; cf. Fig-
 511 ures 3 and 4. The experiments were performed using the Haswell compute nodes (2
 512 sockets with a 16-core Intel Xeon Processor E5-2698 v3 with 2.3 GHz each) of the Cori
 513 supercomputer at NERSC (National Energy Research Scientific Computing Center);
 514 we always employed one processor core per thread. The code was compiled using
 515 Intel 19.0.3.199 compilers and Intel MKL. The subdomain problems and the coarse
 516 problem are solved on one MPI rank using used Pardiso from the Intel MKL with
 517 OpenMP parallelization if more than one OpenMP thread is used.

518 The nonlinear problems are solved using the inexact Newton method with back-
 519 tracking implemented in the Trilinos package NOX up to a relative reduction of the
 520 residual of 10^{-5} . As the linear solver we employ the GMRES (generalized minimal
 521 residual) method [44] from Trilinos AztecOO preconditioned by two-level overlapping
 522 Schwarz domain decomposition preconditioners from Trilinos FROSch (part of the
 523 package ShyLU) as described in section 4; cf. [28, 27, 22, 23, 26]. We iterate the
 524 GMRES method up to a relative reduction of the residual of 10^{-7} for the flow and
 525 temperature problems or 10^{-9} for the coupled problem. Since the number of nonlin-
 526 ear iterations is not influenced by our preconditioners, we always report the number
 527 of linear iterations averaged over the number of Newton iterations.

528 With respect to the Schwarz preconditioners, if not stated otherwise, we will
 529 always use one layer of overlap as determined from the sparsity pattern of the matrix.
 530 On the first level, we apply scaled prolongation operators; cf. subsection 4.2. As
 531 already discussed in [28], we will use two communication steps in order to transfer
 532 information from the first to the second level (scatter and gather); only during the
 533 discussion in subsection 6.1.3, we will also present results using only one or three
 534 communication steps.

535 **6.1. Flow problem for Antarctica.** In this section, we will present an exten-
 536 sive numerical study of GDSW type preconditioners for the land ice flow problem

Without rotational coarse basis functions (2 rigid body modes)								
MPI ranks	GDSW (IS & SF1 & SF2 & CB)				RGDSW (IS & SF1 & SF2 & CB)			
	dim V_0	avg. its (nl its)	avg. setup	avg. solve	dim V_0	avg. its (nl its)	avg. setup	avg. solve
512	4 598	40.8 (11)	15.36 s	12.38 s	1 834	42.6 (11)	14.99 s	12.50 s
1 024	9 306	43.3 (11)	5.80 s	6.27 s	3 740	44.5 (11)	5.65 s	6.08 s
2 048	18 634	41.7 (11)	3.27 s	2.91 s	7 586	42.7 (11)	3.11 s	2.79 s
4 096	37 184	41.4 (11)	2.59 s	2.07 s	15 324	42.5 (11)	1.07 s	1.54 s
8 192	72 964	39.5 (11)	1.51 s	1.84 s	30 620	42.0 (11)	1.20 s	1.16 s
With rotational coarse basis functions (3 rigid body modes)								
MPI ranks	GDSW (IS & SF1 & SF2 & CB)				RGDSW (IS & SF1 & SF2 & CB)			
	dim V_0	avg. its (nl its)	avg. setup	avg. solve	dim V_0	avg. its (nl its)	avg. setup	avg. solve
512	6 897	35.5 (11)	15.77 s	11.21 s	2 751	40.7 (11)	15.23 s	12.22 s
1 024	13 959	35.6 (11)	6.16 s	5.78 s	5 610	42.9 (11)	5.65 s	6.04 s
2 048	27 951	33.5 (11)	3.78 s	3.45 s	11 379	42.2 (11)	3.17 s	2.81 s
4 096	55 776	31.8 (11)	2.21 s	3.80 s	22 986	44.3 (11)	1.95 s	2.70 s
8 192	109 446	29.3 (11)	2.49 s	5.33 s	45 930	40.8 (11)	1.19 s	3.13 s

TABLE 2

Comparison of different coarse spaces for the flow problem on the Antarctica mesh with 4 km horizontal resolution and 20 layers of elements in vertical direction and a total of 35.3 m degrees of freedom. The linear iteration counts (avg. its), setup times (avg. setup), and solve times (avg. solve) are averaged over the number of Newton iterations (nl its). Lowest average iterations counts, setup times, and solve times in each row are marked in **bold**.

# subdomains	512	1 024	2 048	4 096	8 192
GDSW	2 299	4 653	9 317	18 592	36 482
RGDSW	917	1 870	3 793	7 662	15 310

TABLE 3

Number of coarse components Γ_i for the Antarctica mesh with 4 km horizontal resolution. The dimension of the coarse space is the number of coarse components multiplied by the dimension of the null space.

537 for Antarctica. Most of the simulations are performed on a medium size mesh with
538 4 km horizontal resolution and 20 layers of elements in vertical direction. We compare
539 one level Schwarz methods and different GDSW type coarse spaces (subsection 6.1.1)
540 and investigate several reuse strategies (subsection 6.1.2) as well as certain paral-
541 lelization aspects (subsection 6.1.3). Moreover, we investigate the robustness with
542 respect to an increasing number of mesh layers of elements in vertical direction (sub-
543 section 6.1.4), and compare our results using FROSch against the algebraic multigrid
544 package MueLu [4, 3] (subsection 6.1.6).

545 Finally, we provide weak scaling results ranging from the coarsest mesh with
546 16 km horizontal resolution to the finest mesh with 1 km horizontal resolution. The
547 largest computation in this weak scaling study was performed on 32 768 processor
548 cores using 8192 MPI ranks and 4 OpenMP threads per MPI rank solving a problem
549 with more than 566 m degrees of freedom.

550 **6.1.1. Comparison of different Schwarz preconditioners.** First, we com-
551 pare the classical GDSW and the reduced dimension GDSW (RGDSW) coarse spaces
552 in a strong scaling study using both the full three-dimensional null space and a two-
553 dimensional null space where the rotation has been omitted; cf. the discussion in sub-
554 section 4.1. In this study, we reuse the index sets (IS), the symbolic factorizations
555 (SF1 & SF2), and the coarse basis (CB) from the first nonlinear iteration. As can
556 be seen in Table 2, all preconditioners scale numerically, but the iteration counts are

One-level Schwarz						
MPI ranks	one layer of algebraic overlap			two layers of algebraic overlap		
	avg. its (nl its)	avg. setup	avg. solve	avg. its (nl its)	avg. setup	avg. solve
512	67.7 (11)	13.80 s	19.55 s	56.2 (11)	17.95 s	18.40 s
1 024	79.1 (11)	5.00 s	10.60 s	66.5 (11)	6.74 s	10.56 s
2 048	96.1 (11)	1.74 s	6.09 s	80.8 (11)	2.58 s	6.31 s
4 096	113.3 (11)	0.81 s	3.59 s	94.8 (11)	1.21 s	3.99 s
8 192	132.0 (11)	0.47 s	2.15 s	109.5 (11)	0.65 s	2.35 s
RGDSW (IS & SF1 & SF2 & CB & CM)						
MPI ranks	one layer of algebraic overlap			two layers of algebraic overlap		
	avg. its (nl its)	avg. setup	avg. solve	avg. its (nl its)	avg. setup	avg. solve
512	46.7 (11)	14.94 s	13.81 s	42.1 (11)	18.89 s	14.13 s
1 024	49.2 (11)	5.75 s	6.78 s	44.3 (11)	6.95 s	7.21 s
2 048	47.7 (11)	2.92 s	3.10 s	44.3 (11)	2.66 s	3.56 s
4 096	48.9 (11)	0.95 s	1.75 s	45.5 (11)	1.28 s	2.15 s
8 192	50.1 (11)	0.63 s	1.35 s	46.0 (11)	0.76 s	1.66 s

TABLE 4

Comparison of one-level and RGDSW Schwarz preconditioners for the flow problem on the Antarctica mesh with 4 km horizontal resolution and 20 layers of elements in vertical direction and a total of 35.3 m degrees of freedom. The linear iteration counts (avg. its), setup times (avg. setup), and solve times (avg. solve) are averaged over the number of Newton iterations (nl its). Lowest average iterations counts, setup times, and solve times in each row are marked in **bold**.

557 better for the classical GDSW coarse spaces compared to the respective RGDSW
558 coarse spaces. In particular, the best iteration counts are obtained using the classical
559 GDSW coarse space with the full null space. However, the parallel performance is
560 clearly better when reducing the dimension of the coarse space by either omitting the
561 rotational rigid body mode or by using the RGDSW coarse space; see also Table 3 for
562 the number coarse components used in the GDSW and the RGDSW coarse spaces,
563 which, together with the dimension of the employed subspace of the null space, deter-
564 mines the size of the coarse space. In total, the variant with the smallest coarse space,
565 i.e., RGDSW without rotation, yields both the highest iteration counts but the best
566 parallel performance. Hence, we will concentrate on this coarse space in the following
567 experiments.

568 Moreover, we compare one-level and two-level Schwarz methods in Table 4. We
569 observe that the one-level methods do not scale numerically. However, due to the
570 geometry of the ice sheet, the increase in the iteration count of the one-level pre-
571 conditioners is lower compared to usual fully three-dimensional domain decompositions.
572 Due to the reuse strategies for the two-level methods used in this comparison, the
573 setup cost for the one-level preconditioners is only slightly lower; even the coarse ma-
574 trix is reused. However, due to numerical scalability, the two level methods perform
575 clearly better in the solve phase.

576 **6.1.2. Reuse strategies.** In Table 5, we investigate the performance improve-
577 ments due to the use of reuse strategies on the coarse level. As the baseline, we
578 consider reusing the index sets (IS) and the symbolic factorization for the first level
579 (SF1). We then consider reusing only the symbolic factorization of the coarse matrix
580 (SF2) and coarse basis functions (CB) as well as also reusing the coarse matrix itself
581 (CM). As can be observed, the iteration counts increase and, at the same time, the
582 setup cost reduces if parts of the second level are reused. In particular, for lower
583 numbers of MPI ranks and large subdomain problems, the setup cost is significantly

MPI ranks	IS & SF1			IS & SF1 & SF2 & CB			IS & SF1 & SF2 & CB & CM		
	avg. its (nl its)	avg. setup	avg. solve	avg. its (nl its)	avg. setup	avg. its solve	avg. its (nl its)	avg. setup	avg. solve
512	41.9 (11)	25.10 s	12.29 s	42.6 (11)	14.99 s	12.50 s	46.7 (11)	14.94 s	13.81 s
1 024	43.3 (11)	9.18 s	5.85 s	44.5 (11)	5.65 s	6.08 s	49.2 (11)	5.75 s	6.78 s
2 048	41.4 (11)	4.15 s	2.63 s	42.7 (11)	3.11 s	2.79 s	47.7 (11)	2.92 s	3.10 s
4 096	41.2 (11)	1.66 s	1.49 s	42.5 (11)	1.07 s	1.54 s	48.9 (11)	0.95 s	1.75 s
8 192	40.2 (11)	1.26 s	1.06 s	42.0 (11)	1.20 s	1.16 s	50.1 (11)	0.63 s	1.35 s

TABLE 5

Comparison of different reuse strategies for the two-level RGDSW Schwarz preconditioner for the flow problem on the Antarctica mesh with 4 km horizontal resolution and 20 layers of elements in vertical direction and a total of 35.3 m degrees of freedom. The linear iteration counts (avg. its), setup times (avg. setup), and solve times (avg. solve) are averaged over the number of Newton iterations (nl its). Lowest average iterations counts, setup times, and solve times in each row are marked in **bold**.

MPI ranks	1 comm. step		2 comm. step		3 comm. step	
	avg. setup	avg. solve	avg. setup	avg. solve	avg. setup	avg. solve
512	15.38 s	13.8 s	14.99 s	12.50 s	15.75 s	13.85 s
1 024	5.68 s	6.25 s	5.65 s	6.08 s	5.63 s	6.10 s
2 048	2.91 s	3.27 s	2.94 s	2.78 s	3.40 s	2.75 s
4 096	1.35 s	3.77 s	1.07 s	1.54 s	1.15 s	1.56 s
8 192	2.5 s	12.22 s	1.29 s	1.13 s	1.29 s	1.17 s

TABLE 6

Variation of the number of communication steps for the scatter and gather operations on the coarse level for the RGDSW Schwarz preconditioner for the flow problem on the Antarctica mesh with 4 km horizontal resolution and 20 layers of elements in vertical direction and a total of 35.3 m degrees of freedom. The linear iteration counts (avg. its), setup times (avg. setup), and solve times (avg. solve) are averaged over the number of Newton iterations (nl its). Lowest average iterations counts, setup times, and solve times in each row are marked in **bold**.

584 reduced. Due to the better overall performance, we will only consider results using IS
585 & SF1 & SF2 & CB or IS & SF1 & SF2 & CB & CM for the following results using
586 two-level preconditioners for the flow problem.

587 **6.1.3. Parallelization aspects.** Here, we discuss two parallelization aspects.

588 First, we discuss the communication between all MPI ranks and the single MPI
589 rank which computes the coarse problem, the *coarse rank*. In particular, both all-to-
590 one and one-to-all communication patterns are necessary in our implementation: In
591 the setup phase, the coarse matrix, which is computed by an RAP product on all MPI
592 ranks, has to be communicated to the coarse rank. Then, in each linear iteration of the
593 solve phase, the right hand side of the coarse problem has to be communicated from
594 all ranks to the coarse rank and the corresponding solution has to be communicated
595 back. As already discussed in [28, section 4.7], this type of communication does not
596 perform well for large numbers of MPI ranks using the Trilinos import and export
597 objects. In [28, section 4.7] Epetra import and export objects were employed, whereas
598 their Tpetra counterparts are considered here. Therefore, we introduce nested sets
599 of MPI ranks, beginning with all MPI ranks and ending with the single coarse rank,
600 and perform the all-to-one and one-to-all communication using multiple steps; cf. [28,
601 section 4.7] for a more detailed discussion.

602 In Table 6, we present corresponding results, varying the number of communica-
603 tion steps between one to three. As can be observed, using two or three communication
604 steps, we obtain good the parallel scalability. However, if only a single import/export

cores	OpenMP parallelization (512 MPI ranks)			MPI parallelization				
	OpenMP threads	avg. its (nl its)	avg. setup	avg. solve	MPI ranks	avg. its (nl its)	avg. setup	avg. its solve
512	1	42.6 (11)	14.99 s	12.50 s	512	42.6 (11)	14.99 s	12.50 s
1 024	2	42.6 (11)	9.43 s	6.80 s	1 024	44.5 (11)	5.65 s	6.08 s
2 048	4	42.6 (11)	5.50 s	4.02 s	2 048	42.7 (11)	3.11 s	2.79 s
4 096	8	42.6 (11)	3.65 s	2.71 s	4 096	42.5 (11)	1.07 s	1.54 s
8 192	16	42.6 (11)	2.56 s	2.32 s	8 192	42.0 (11)	1.20 s	1.16 s

TABLE 7

Comparison of increasing the numbers of OpenMP threads or MPI ranks for the RGDSW Schwarz preconditioner for the flow problem on the Antarctica mesh with 4 km horizontal resolution and 20 layers of elements in vertical direction and a total of 35.3 m degrees of freedom. The linear iteration counts (avg. its), setup times (avg. setup), and solve times (avg. solve) are averaged over the number of Newton iterations (nl its). Lowest average iterations counts, setup times, and solve times in each row are marked in **bold**.

# layers	# dofs	Constant number of MPI ranks				128 MPI ranks per 5 layers			
		MPI ranks	avg. its (nl its)	avg. setup	avg. solve	MPI ranks	avg. its (nl its)	avg. setup	avg. solve
5	10.1 m		39.2 (11)	0.42 s	0.58 s	128	38.8 (12)	5.47 s	7.79 s
10	18.5 m		41.0 (11)	0.79 s	1.15 s	256	37.8 (11)	8.46 s	8.57 s
20	35.3 m	2 048	42.7 (11)	2.94 s	2.78 s	512	42.6 (11)	14.99 s	12.50 s
40	69.0 m		45.6 (12)	5.77 s	6.67 s	1 024	47.8 (12)	19.00 s	15.72 s
80	136.3 m		45.3 (15)	14.41 s	14.53 s	2 048	45.3 (15)	14.41 s	14.53 s

TABLE 8

Performance of the RGDSW Schwarz preconditioner for an increasing number of layers for the flow problem on the Antarctica mesh with 4 km horizontal resolution and 20 layers of elements in vertical direction. Left: constant number of MPI ranks and subdomains. Right: increasing the number of MPI ranks and subdomains proportional to the number of layers. The linear iteration counts (avg. its), setup times (avg. setup), and solve times (avg. solve) are averaged over the number of Newton iterations (nl its).

605 call from Tpetra is performed in each scatter/gather operation, the parallel scalabil-
 606 ity deteriorates due to a significant communication overhead. In particular, the solve
 607 time, where one scatter and one gather operation is performed in each linear iteration,
 608 is increased significantly. Hence, in all other experiments, we use two communication
 609 steps.

610 In Table 7, we compare OpenMP parallelization and MPI parallelization. Starting
 611 with 512 MPI ranks, we increase the number of processor cores up to 8 192 using
 612 either OpenMP threads or a higher number of MPI ranks. As can be observed, MPI
 613 parallelization is clearly superior in this comparison even though the size of the coarse
 614 problem increases with an increasing number of MPI ranks and subdomains, whereas
 615 it stays constant for OpenMP parallelization. Only for large numbers of MPI ranks
 616 and subdomains, it may be reasonable to additionally use OpenMP parallelization
 617 since it does not further increase the coarse problem size. Alternatively, more levels
 618 could be added to the the GDSW type preconditioners; cf. [29, 30]. Hence, we will
 619 restrict ourselves to using MPI parallelization; only in the largest weak scalability
 620 study in subsection 6.1.5, we also show results using OpenMP parallelization in
 621 addition to MPI parallelization.

622 6.1.4. Increasing the number of layers of elements in vertical direction.

623 In most of our numerical simulations, we use 20 layers of elements in vertical direction;
 624 this corresponds to a rather fine resolution in vertical direction, which would also be
 625 used in production runs of the land ice simulations. However, we are also interested in

1 OpenMP thread								
MPI ranks	mesh	# dofs	IS & SF1 & SF2 & CB			IS & SF1 & SF2 & CB & CM		
			avg. its (nl its)	avg. setup	avg. solve	avg. its (nl its)	avg. setup	avg. solve
32	16 km	2.2 m	24.1 (11)	11.97 s	9.47 s	24.0 (11)	11.18 s	9.45 s
128	8 km	8.8 m	32.0 (10)	14.08 s	8.71 s	32.6 (10)	14.06 s	8.93 s
512	4 km	35.3 m	42.6 (11)	14.99 s	12.50 s	42.6 (11)	16.14 s	14.19 s
2 048	2 km	141.5 m	61.0 (11)	22.83 s	19.76 s	67.1 (11)	22.65 s	21.69 s
8 192	1 km	566.1 m	67.1 (14)	17.36 s	22.91 s	73.0 (14)	16.80 s	28.48 s
4 OpenMP threads								
MPI ranks	mesh	# dofs	IS & SF1 & SF2 & CB			IS & SF1 & SF2 & CB & CM		
			avg. its (nl its)	avg. setup	avg. solve	avg. its (nl its)	avg. setup	avg. solve
32	16 km	2.2 m	23.5 (11)	4.15 s	3.25 s	23.8 (11)	3.93 s	3.28 s
128	8 km	8.8 m	32.0 (10)	4.97 s	2.85 s	32.6 (10)	4.62 s	2.82 s
512	4 km	35.3 m	42.6 (11)	5.50 s	4.02 s	46.7 (11)	5.27 s	4.45 s
2 048	2 km	141.5 m	61.0 (11)	7.36 s	6.55 s	67.1 (11)	7.15 s	7.34 s
8 192	1 km	566.1 m	67.1 (14)	6.20 s	7.39 s	73.0 (14)	5.75 s	7.92 s

TABLE 9

Weak scalability studies for the RGDSW Schwarz preconditioner for the flow problem on the Antarctica mesh with 4 km horizontal resolution and 20 layers of elements in vertical direction. We consider the cases of 1 OpenMP thread (top) and 4 OpenMP threads (bottom) per MPI rank as well as IS & SF1 & SF2 & CB (left) and IS & SF1 & SF2 & CB & CM (right) reuse strategies. The linear iteration counts (avg. its), setup times (avg. setup), and solve times (avg. solve) are averaged over the number of Newton iterations (nl its). Lowest average iterations counts, setup times, and solve times in each row are marked in **bold**.

626 investigating the influence of an increasing number of layers on the performance of our
627 preconditioners. In Table 8, we employ the RGDSW preconditioner and fix the top
628 surface mesh while increasing the number of vertical layers of elements from 5 up to 80.
629 For both cases, keeping the number of MPI ranks fixed and increasing it proportional
630 to the number of layers, the iterations counts are very robust. However, the number of
631 nonlinear iterations increases slightly from 11 to 15. Note that we use 2048 MPI ranks
632 for all problems in this experiment when we keep constant number of MPI ranks. This
633 also allows comparing scalability of the solver for different problems to 2048 ranks.
634 For example, even the 5 layer problem achieves 13.4x speedup in average solve going
635 from 128 MPI ranks to 2048 MPI ranks demonstrating good parallel scalability.

636 **6.1.5. Weak scaling.** In Table 9, we provide four weak scalability studies, where
637 we increase the number of MPI ranks proportional to the resolution of the top surface
638 mesh; the number of vertical layers is again fixed to 20. In particular, we consider 1
639 or 4 OpenMP threads per MPI rank combined with the IS & SF1 & SF2 & CB and
640 IS & SF1 & SF2 & CB & CM reuse strategies; cf. subsections 4.5 and 6.1.2.

641 We observe good weak scalability from 32 to 8 192 (1 OpenMP thread per MPI
642 rank) and from 128 to 32 768 (4 OpenMP threads per MPI rank) processor cores.
643 However, there is a moderate increase in the number of iterations, which is most
644 likely caused by the unstructured domain decomposition, where subdomains with
645 irregular shape and bad aspect ratio may occur in certain cases, in particular, at the
646 boundary of the top surface mesh; cf. Figure 3. For all configurations, the setup time
647 scales very well, whereas the increase in the solve time is more pronounced; however,
648 except for the case of 1 OpenMP rank and IS & SF1 & SF2 & CB & CM reuse, the
649 solve times does increase clearly less than the number of iterations.

650 Generally, we observe a speedup by a factor of approximately 3 when using 4
651 threads instead of 1 OpenMP thread. However, the former uses 4 times the number

MPI ranks	FROSch						MueLu		
	IS & SF1			IS & SF1 & SF2 & CB & CM			Vertical Semi-Coarsening		
	avg. its (nl its)	avg. setup	avg. solve	avg. its (nl its)	avg. setup	avg. solve	avg. its (nl its)	avg. setup	avg. solve
512	41.9 (11)	25.10 s	12.29 s	46.7 (11)	14.94 s	13.81 s	31.0 (11)	0.35 s	3.00 s
1024	43.3 (11)	9.18 s	5.85 s	49.2 (11)	5.75 s	6.78 s	30.7 (11)	0.32 s	1.66 s
2048	41.4 (11)	4.15 s	2.63 s	47.7 (11)	2.92 s	3.10 s	31.0 (11)	0.36 s	1.02 s
4096	41.2 (11)	1.66 s	1.49 s	48.9 (11)	0.95 s	1.75 s	30.9 (11)	0.80 s	1.69 s
8192	40.2 (11)	1.26 s	1.06 s	50.1 (11)	0.63 s	1.35 s	48.5 (11)	1.05 s	2.55 s

TABLE 10

Comparison of the RGDSW Schwarz preconditioner with two different reuse strategies against MueLu algebraic multigrid for the flow problem on the Antarctica mesh with 4 km horizontal resolution and 20 layers of elements in vertical direction and a total of 35.3 m degrees of freedom. The linear iteration counts (avg. its), setup times (avg. setup), and solve times (avg. solve) are averaged over the number of Newton iterations (nl its). Lowest average iterations counts, setup times, and solve times in each row are marked in **bold**.

of cores compared to the latter. Hence, OpenMP parallelization has to be carefully considered with respect to the size of the problems and the available parallelism.

6.1.6. Comparison against multigrid. As a final result for the velocity problem for Antarctica, we compare the strong scalability for the RGDSW preconditioner in the FROSch package to an algebraic multigrid preconditioner described in [50] and using MueLu. The method uses a vertical semi-coarsening approach designed for the ice sheet problems. As can be observed in Table 10, for small numbers of MPI ranks and subdomains, the total time is clearly higher for FROSch compared to MueLu. This is caused by the superlinear complexity of the direct solvers which are used to solve the problems on the overlapping subdomains. However, when increasing the number of subdomains and therefore reducing the size of the overlapping subdomains, we observe a better speedup compared to MueLu. We note that MueLu settings were not fine-tuned for this particular problem. However, it is fair to say that FROSch is competitive for large number of sub-domains especially considering the fact that FROSch is used almost as a black box.

6.2. Temperature problem for Greenland. As a second problem for land ice simulations, we consider the temperature problem described in subsection 2.2 for Greenland; see also Figure 4. In Table 11, we compare one-level Schwarz preconditioners and RGDSW preconditioner using one and two layers of algebraic overlap. As can be observed, already the one-level methods scale well since all subdomains are adjacent to the Dirichlet boundary, which is the whole upper surface; cf. subsection 2.2. Due to the lower setup and application cost of the one-level method, both the setup and the solve times are also lower. Therefore, one-level Schwarz methods are very well suited for solving the temperature problem, and hence, it is not necessary to add a second level. Note that the standalone steady-state temperature problem is not physically meaningful because the temperature equilibration is on time scales that are much larger than the velocity ones. For this reason, we focus our attention on the coupled problem.

6.3. Coupled problem for Greenland. Finally, we consider the coupled problem for the non-uniform Greenland meshes and present, for the first time, results for scalable monolithic two-level preconditioners for this problem. Note that the nonlinear iteration is very sensitive for the coupled problem. In particular, even though a very strict stopping tolerance of 10^{-9} is used for the GMRES iteration, changing the

One-level Schwarz						
MPI ranks	one layer of algebraic overlap			two layers of algebraic overlap		
	avg. its	avg. setup	avg. solve	avg. its	avg. setup	avg. solve
512	18.1 (11)	0.42 s	0.35 s	17.1 (11)	0.51 s	0.40 s
1 024	23.7 (11)	0.25 s	0.25 s	22.1 (11)	0.27 s	0.27 s
2 048	29.6 (11)	0.16 s	0.17 s	27.6 (11)	0.23 s	0.20 s
4 096	39.8 (11)	0.15 s	0.15 s	35.6 (11)	0.17 s	0.17 s
RGDSW (IS & SF1 & SF2 & CB)						
MPI ranks	one layer of algebraic overlap			two layers of algebraic overlap		
	avg. its	avg. setup	avg. solve	avg. its	avg. setup	avg. solve
512	19.5 (11)	0.44 s	0.41 s	18.7 (11)	0.55 s	0.46 s
1 024	25.2 (11)	0.28 s	0.29 s	23.9 (11)	0.35 s	0.33 s
2 048	31.5 (11)	0.26 s	0.24 s	29.5 (11)	0.25 s	0.27 s
4 096	42.2 (11)	0.25 s	0.27 s	38.2 (11)	0.25 s	0.29 s

TABLE 11

Comparison of one-level and RGDSW Schwarz preconditioners for the temperature problem on the Greenland mesh with 1-10km horizontal resolution (fine mesh) and 20 layers of elements in vertical direction and a total of 1.9m degrees of freedom. The linear iteration counts (avg. its), setup times (avg. setup), and solve times (avg. solve) are averaged over the number of Newton iterations (nl its). Lowest average iterations counts, setup times, and solve times in each row are marked in **bold**.

fully coupled extensions							
MPI ranks	dim V_0	NR			IS & CB		
		avg. its (nl its)	avg. setup	avg. solve	avg. its (nl its)	avg. setup	avg. solve
256	1 400	100.1 (27)	4.10 s	6.40 s	18.5 (70)	2.28 s	1.07 s
512	2 852	129.1 (28)	1.88 s	4.20 s	24.6 (38)	1.04 s	0.70 s
1 024	6 036	191.2 (65)	1.21 s	4.76 s	34.2 (32)	0.66 s	0.70 s
2 048	12 368	237.4 (30)	0.96 s	4.06 s	37.3 (30)	0.60 s	0.58 s
decoupled extensions							
MPI ranks	dim V_0	NR			IS & CB		
		avg. its (nl its)	avg. setup	avg. solve	avg. its (nl its)	avg. setup	avg. solve
256	1 400	23.6 (29)	3.90 s	1.32 s	21.5 (34)	2.23 s	1.18 s
512	2 852	27.5 (30)	1.83 s	0.78 s	26.4 (33)	1.13 s	0.78 s
1 024	6 036	30.1 (29)	1.19 s	0.60 s	28.6 (43)	0.66 s	0.61 s
2 048	12 368	36.4 (30)	0.69 s	0.56 s	31.2 (50)	0.57 s	0.55 s

TABLE 12

Comparison of monolithic RGDSW Schwarz preconditioners with different coarse spaces neglecting rotational coarse basis functions for the velocity degrees of freedom for the coupled problem on the Greenland mesh with 3-30km horizontal resolution (coarse mesh) and 20 layers of elements in vertical direction and a total of 7.5m degrees of freedom. The linear iteration counts (avg. its), setup times (avg. setup), and solve times (avg. solve) are averaged over the number of Newton iterations (nl its). Lowest average iterations counts, setup times, and solve times in each row are marked in **bold**.

685 preconditioner may result in significant variations in the number of nonlinear itera-
686 tions; cf. Tables 12, 13, 15, and 16. Note again that, in this work, we report linear
687 iteration counts averaged over the total number of Newton iterations, so that our
688 results are not influenced much by the sensitivity of the nonlinear solver.

689 First, we compare different monolithic coarse spaces for a coarse Greenland mesh
690 with 3-30 km horizontal resolution, 20 layers of elements in vertical direction, and a
691 total of more than 7.5 m degrees of freedom. In order to focus only on the coarse basis,
692 we only consider two following reuse strategies. On the one hand, we do not reuse any

fully coupled extensions							
MPI ranks	dim V_0	NR			IS & CB		
		avg. its (nl its)	avg. setup	avg. solve	avg. its (nl its)	avg. setup	avg. solve
256	1 750	99.3 (27)	4.20 s	6.35 s	21.9 (30)	2.35 s	1.22 s
512	3 565	131.4 (28)	1.95 s	4.40 s	22.8 (50)	1.09 s	0.66 s
1 024	7 545	261.7 (31)	1.22 s	5.47 s	31.3 (29)	0.73 s	0.61 s
2 048	15 460	325.7 (27)	1.08 s	8.53 s	41.7 (25)	0.74 s	1.16 s
decoupled extensions							
MPI ranks	dim V_0	NR			IS & CB		
		avg. its (nl its)	avg. setup	avg. solve	avg. its (nl its)	avg. setup	avg. solve
256	1 750	22.0 (28)	3.98 s	1.23 s	22.8 (27)	2.23 s	1.28 s
512	3 565	24.7 (32)	1.92 s	0.72 s	23.8 (39)	1.11 s	0.69 s
1 024	7 545	31.9 (27)	1.23 s	0.62 s	33.1 (27)	0.74 s	0.76 s
2 048	15 460	31.2 (38)	0.99 s	0.77 s	34.7 (34)	0.69 s	1.05 s

TABLE 13

Comparison of monolithic RGDSW Schwarz preconditioners with different coarse spaces including rotational coarse basis functions for the velocity degrees of freedom for the coupled problem on the Greenland mesh with 3-30 km horizontal resolution (coarse mesh) and 20 layers of elements in vertical direction and a total of 7.5 m degrees of freedom. The linear iteration counts (avg. its), setup times (avg. setup), and solve times (avg. solve) are averaged over the number of Newton iterations (nl its). Lowest average iterations counts, setup times, and solve times in each row are marked in **bold**.

# subdomains		256	512	1 024	2 048	4 096
RGDSW	3-30 km	350	713	1 509	3 092	6 245
	1-10 km	-	721	1 536	3 230	6 615

TABLE 14

Number of coarse components Γ_i for the two non-uniform Greenland meshes with 3-30 km and 1-10 km horizontal resolution. The dimension of the coarse space is the number of coarse components multiplied by the dimension of the null space.

693 information from the first Newton iteration (NR), on the other hand, we only reuse
694 index sets and the coarse basis (IS & CB); in both cases, we do not reuse symbolic
695 factorizations because of variations in the sparsity pattern of the system matrix. In
696 combination with these two reuse strategies, we consider monolithic RGDSW pre-
697 conditioners (see subsection 4.3) with fully coupled extensions using (4.10) and decoupled
698 extensions using (4.12), respectively. As in subsection 6.1.1, we consider neglecting the
699 rotational coarse basis functions and including the rotational coarse basis functions
700 for the velocity part in Table 12 and Table 13, respectively. We clearly observe that
701 using the standard monolithic coarse space (without reuse of the coarse basis func-
702 tions) does not yield a scalable two-level method. Adding the rotational coarse basis
703 function even yields higher iterations counts compared to neglecting rotational coarse
704 basis functions. However, using the decoupled extensions described in subsection 4.3
705 instead, we obtain a scalable monolithic RGDSW preconditioner. Moreover, it seems
706 that the coupling terms in the first Newton iteration do not deteriorate the scalability.
707 Hence, reusing the coarse basis from the first Newton iteration even yields a scalable
708 preconditioner for both cases, the fully coupled and the decoupled extensions.

709 Moreover, as for the velocity problem (see subsection 6.1.1), the time to solution
710 is lower when neglecting the rotational coarse basis functions due to the lower coarse
711 space dimension; see also Table 14 for the numbers of interface components. Conse-
712 quently, we will only consider the case of neglecting rotational coarse basis functions
713 for the monolithic RGDSW coarse spaces in the following experiments.

MPI ranks	decoupled (NR)			fully coupled (IS & CB)			decoupled (IS & SF1 & CB)		
	avg. (nl its)	avg. setup	avg. solve	avg. (nl its)	avg. setup	avg. solve	avg. (nl its)	avg. setup	avg. solve
512	41.3 (36)	18.78 s	4.99 s	45.3 (32)	11.84 s	5.35 s	45.0 (35)	10.53 s	5.36 s
1 024	53.0 (29)	8.68 s	4.22 s	47.8 (37)	5.36 s	3.82 s	54.3 (32)	4.59 s	4.31 s
2 048	62.2 (86)	4.47 s	4.23 s	66.7 (38)	2.81 s	4.53 s	59.1 (38)	2.32 s	3.99 s
4 096	68.9 (40)	2.52 s	2.86 s	79.1 (36)	1.61 s	3.30 s	78.7 (38)	1.37 s	3.30 s

TABLE 15

Comparison of monolithic RGDSW Schwarz preconditioners with different reuse strategies for the coupled problem on the Greenland mesh with 1-10 km horizontal resolution (fine mesh) and 20 layers of elements in vertical direction and a total of 68.6 m degrees of freedom. The linear iteration counts (avg. its), setup times (avg. setup), and solve times (avg. solve) are averaged over the number of Newton iterations (nl its). Lowest average iterations counts, setup times, and solve times in each row are marked in **bold**.

One-level Schwarz (NR)						
MPI ranks	$\delta = 1h$			$\delta = 2h$		
	avg. its (nl its)	avg. setup	avg. solve	avg. its (nl its)	avg. setup	avg. solve
512	48.7 (35)	11.3 s	5.41 s	42.6 (33)	15.2 s	5.80 s
1 024	61.9 (40)	5.29 s	4.75 s	58.8 (30)	6.92 s	5.48 s
2 048	89.9 (30)	2.52 s	5.70 s	73.5 (34)	3.83 s	6.24 s
4 096	116.1 (31)	1.17 s	3.68 s	103.1 (33)	1.86 s	4.87 s
One-level Schwarz (NR & SF1)						
MPI ranks	$\delta = 1h$			$\delta = 2h$		
	avg. its (nl its)	avg. setup	avg. solve	avg. its (nl its)	avg. setup	avg. solve
512	52.2 (32)	10.16 s	5.88 s	42.6 (39)	13.80 s	5.77 s
1 024	66.2 (35)	4.32 s	4.91 s	35.7 (72)	5.98 s	3.19 s
2 048	82.0 (37)	2.07 s	5.27 s	68.5 (39)	3.20 s	5.81 s
4 096	120.39 (31)	0.92 s	3.83 s	95.5 (32)	1.48 s	4.53 s

TABLE 16

Strong scaling study for monolithic one-level Schwarz preconditioners with one or two layers of algebraic overlap for the coupled problem on the Greenland mesh with 1-10 km horizontal resolution (fine mesh) and 20 layers of elements in vertical direction and a total of 68.6 m degrees of freedom. The linear iteration counts (avg. its), setup times (avg. setup), and solve times (avg. solve) are averaged over the number of Newton iterations (nl its). Lowest average iterations counts, setup times, and solve times in each row are marked in **bold**.

714 Next, we investigate different reuse strategies in Table 15 for a fine Greenland
715 mesh with 1-10 km horizontal resolution, 20 layers of elements in vertical direction,
716 and a total of more than 68 m degrees of freedom. As can be observed, the best
717 parallel performance can be obtained when reusing the index sets (IS) as well as the
718 symbolic factorization on the first level (SF1) and the coarse basis (CB) from the first
719 Newton iteration. Note that reusing the symbolic factorization on the second level,
720 the iteration counts always deteriorated in our experiments.

721 Finally, we also provide results for monolithic one-level Schwarz preconditioners in
722 comparison to the two-level monolithic RGDSW preconditioner. As can be observed
723 in Table 16, the iteration counts for the one-level preconditioners with one level of
724 overlap are clearly higher compared to the RGDSW preconditioner with one layer of
725 overlap in Table 15. Therefore, the solve time is reduced by adding an appropriate
726 second level. On the other hand, the setup cost for the two-level methods is again
727 higher; in particular, the additional coarse problem is also a fully coupled multi-
728 physics problem in this case. The computing time for an overlap of two layers was
729 higher for both the one-level and the two-level method.

730 Note that we observed that the matrix structure of the coupled problem is not
731 well-suited for OpenMP parallelization of the node-level solver Pardiso. In particular,
732 the speedup was always lower than a factor of 2 when using 4 OpenMP threads and
733 one processor core per OpenMP thread. For the case of 4 096 MPI ranks, the speedup
734 was even reduced to a factor of less than 1.2.

735 **7. Conclusions.** We have presented a flexible preconditioning framework based
736 on the GDSW method, which yields scalable and robust preconditioners for all con-
737 sidered land ice problems. In particular, the implementation of this framework in
738 FROSch can be applied out-of-the-box; between the different problems, only minor
739 changes of the input parameters are necessary. Moreover, to the best of our knowl-
740 edge, we have presented the first scalable two-level method for the coupled problem
741 for land ice simulations. Compared to the single physics problems, the extension
742 operators have to be decoupled, which can easily be done by changing one
743 parameter in FROSch. Otherwise, the coarse basis from the first Newton iteration
744 also resulted in a scalable method.

745 The parallel results of several strong and weak scaling studies, involving different
746 coarse space variants and reuse strategies as well as OpenMP parallelization and MPI
747 communication aspects, prove both the robustness and numerical scalability of the
748 methods as well as the parallel scalability of the implementation in FROSch.

749 Furthermore, we have observed that the direct solvers in our two-level method
750 are the main bottleneck. On one hand, the direct solvers on the first level determine
751 the computing time for a small number of MPI ranks and large subdomain problems.
752 On the other hand, the direct solver on the coarse level may become the scaling
753 bottleneck for very large numbers of MPI ranks and subdomains. The improvement
754 of the subdomain and coarse solvers for these complex problems will be subject of
755 future research.

756 **Acknowledgments.** Support for this work was provided through the SciDAC
757 projects FASTMath and ProSPect, funded by the U.S. Department of Energy (DOE)
758 Office of Science, Advanced Scientific Computing Research and Biological and Envi-
759 ronmental Research programs. This research used resources of the National Energy
760 Research Scientific Computing Center (NERSC), a U.S. Department of Energy Office
761 of Science User Facility operated under Contract No. DE-AC02-05CH11231.

762 **Disclaimer.** This paper describes objective technical results and analysis. Any
763 subjective views or opinions that might be expressed in the paper do not necessarily
764 represent the views of the U.S. Department of Energy or the United States Govern-
765 ment.

766

REFERENCES

- 767 [1] A. ASCHWANDEN, E. BUELER, C. KHROULEV, AND H. BLATTER, *An enthalpy formulation for*
768 *glaciers and ice sheets*, Journal of Glaciology, 58 (2012), pp. 441–457, [https://doi.org/doi:](https://doi.org/doi:10.3189/2012JoG11J088)
769 [10.3189/2012JoG11J088](https://doi.org/doi:10.3189/2012JoG11J088).
- 770 [2] E. BAVIER, M. HOEMMEN, S. RAJAMANICKAM, AND H. THORNQUIST, *Amesos2 and belos: Direct*
771 *and iterative solvers for large sparse linear systems*, Scientific Programming, 20 (2012),
772 pp. 241–255.
- 773 [3] L. BERGER-VERGIAT, C. A. GLUSA, J. J. HU, M. MAYR, A. PROKOPENKO, C. M. SIEFERT,
774 R. S. TUMINARO, AND T. A. WIESNER, *MueLu multigrid framework*. [http://trilinos.org/](http://trilinos.org/packages/muelu)
775 [packages/muelu](http://trilinos.org/packages/muelu), 2019.
- 776 [4] L. BERGER-VERGIAT, C. A. GLUSA, J. J. HU, M. MAYR, A. PROKOPENKO, C. M. SIEFERT,
777 R. S. TUMINARO, AND T. A. WIESNER, *MueLu user's guide*, Tech. Report SAND2019-
778 0537, Sandia National Laboratories, 2019.

- 779 [5] D. J. BRINKERHOFF AND J. V. JOHNSON, *Data assimilation and prognostic whole ice sheet*
780 *modelling with the variationally derived, higher order, open source, and fully parallel ice*
781 *sheet model varglas*, *The Cryosphere*, 7 (2013), pp. 1161–1184, [https://doi.org/10.5194/](https://doi.org/10.5194/tc-7-1161-2013)
782 [tc-7-1161-2013](https://tc.copernicus.org/articles/7/1161/2013/), <https://tc.copernicus.org/articles/7/1161/2013/>.
- 783 [6] J. BROWN, B. SMITH, AND A. AHMADIA, *Achieving textbook multigrid efficiency for hydrostatic*
784 *ice sheet flow*, *SIAM Journal on Scientific Computing*, 35 (2013), pp. B359–B375, <https://doi.org/10.1137/110834512>, <https://doi.org/10.1137/110834512>, [https://arxiv.org/abs/](https://arxiv.org/abs/https://doi.org/10.1137/110834512)
785 <https://doi.org/10.1137/110834512>.
- 786 [7] M. BUCK, O. ILIEV, AND H. ANDRÄ, *Multiscale finite elements for linear elasticity: Oscillatory*
787 *boundary conditions*, in *Domain Decomposition Methods in Science and Engineering XXI*,
788 vol. 98 of LNCSE, Springer, 2014, pp. 237–245.
- 789 [8] X.-C. CAI AND M. SARKIS, *A restricted additive Schwarz preconditioner for general sparse*
790 *linear systems*, *SIAM J. Sci. Comput.*, 21 (1999), pp. 792–797.
- 791 [9] L. CAMBIER, C. CHEN, E. G. BOMAN, S. RAJAMANICKAM, R. S. TUMINARO, AND E. DARVE,
792 *An algebraic sparsified nested dissection algorithm using low-rank approximations*, *SIAM*
793 *Journal on Matrix Analysis and Applications*, 41 (2020), pp. 715–746.
- 794 [10] C. CHEN, L. CAMBIER, E. G. BOMAN, S. RAJAMANICKAM, R. S. TUMINARO, AND E. DARVE, *A*
795 *robust hierarchical solver for ill-conditioned systems with applications to ice sheet modeling*,
796 *Journal of Computational Physics*, 396 (2019), pp. 819–836.
- 797 [11] J. CHURCH, P. CLARK, A. CAZENAVE, J. GREGORY, S. JEVREJEVA, A. LEVERMANN, M. MER-
798 *rifield*, G. MILNE, R. NEREM, P. NUNN, A. PAYNE, W. PFEFFER, D. STAMMER, AND
799 A. UNNIKRISSNAN, *Sea Level Change*, Cambridge University Press, Cambridge, United
800 Kingdom and New York, NY, USA, 2013, book section 13, pp. 1137–1216, [https://doi.org/](https://doi.org/10.1017/CBO9781107415324.026)
801 [10.1017/CBO9781107415324.026](https://doi.org/10.1017/CBO9781107415324.026), www.climatechange2013.org.
- 802 [12] C. R. DOHRMANN, A. KLAWONN, AND O. B. WIDLUND, *Domain decomposition for less regular*
803 *subdomains: overlapping Schwarz in two dimensions*, *SIAM J. Numer. Anal.*, 46 (2008),
804 pp. 2153–2168.
- 805 [13] C. R. DOHRMANN, A. KLAWONN, AND O. B. WIDLUND, *A family of energy minimizing coarse*
806 *spaces for overlapping Schwarz preconditioners*, in *Domain decomposition methods in sci-*
807 *ence and engineering XVII*, vol. 60 of *Lect. Notes Comput. Sci. Eng.*, Springer, Berlin,
808 2008, pp. 247–254.
- 809 [14] C. R. DOHRMANN AND O. B. WIDLUND, *An overlapping schwarz algorithm for almost incom-*
810 *pressible elasticity*, *SIAM J. Numer. Anal.*, 47 (2009), pp. 2897–2923.
- 811 [15] C. R. DOHRMANN AND O. B. WIDLUND, *An alternative coarse space for irregular subdomains*
812 *and an overlapping Schwarz algorithm for scalar elliptic problems in the plane*, *SIAM J.*
813 *Numer. Anal.*, 50 (2012), pp. 2522–2537, <https://doi.org/10.1137/110853959>, [https://doi.](https://doi.org/10.1137/110853959)
814 [org/10.1137/110853959](https://doi.org/10.1137/110853959).
- 815 [16] C. R. DOHRMANN AND O. B. WIDLUND, *On the design of small coarse spaces for domain*
816 *decomposition algorithms*, *SIAM J. Sci. Comput.*, 39 (2017), pp. A1466–A1488.
- 817 [17] E. EFSTATHIOU AND M. J. GANDER, *Why restricted additive Schwarz converges faster than*
818 *additive Schwarz*, *BIT*, 43 (2003), pp. 945–959.
- 819 [18] O. GAGLIARDINI, T. ZWINGER, F. GILLET-CHAULET, G. DURAND, L. FAVIER, B. DE FLEURIAN,
820 R. GREVE, M. MALINEN, C. MARTÍN, P. RÅBACK, J. RUOKOLAINEN, M. SACCHET-
821 *tini*, M. SCHÄFER, H. SEDDIK, AND J. THIES, *Capabilities and performance of*
822 *Elmer/Ice, a new-generation ice sheet model*, *Geoscientific Model Development*, 6 (2013),
823 pp. 1299–1318, <https://doi.org/10.5194/gmd-6-1299-2013>, [http://www.geosci-model-dev.](http://www.geosci-model-dev.net/6/1299/2013/)
824 [net/6/1299/2013/](http://www.geosci-model-dev.net/6/1299/2013/).
- 825 [19] F. HABBAL, E. LAROUB, M. MORLIGHEM, H. SEROUSSI, C. P. BORSTAD, AND E. RIGNOT, *Opti-*
826 *mal numerical solvers for transient simulations of ice flow using the ice sheet system model*
827 *(issm versions 4.2.5 and 4.11)*, *Geoscientific Model Development*, 10 (2017), pp. 155–
828 168, <https://doi.org/10.5194/gmd-10-155-2017>, [https://gmd.copernicus.org/articles/10/](https://gmd.copernicus.org/articles/10/155/2017/)
829 [155/2017/](https://gmd.copernicus.org/articles/10/155/2017/).
- 830 [20] A. HEINLEIN, *Parallel Overlapping Schwarz Preconditioners and Multiscale Discretizations with*
831 *Applications to Fluid-Structure Interaction and Highly Heterogeneous Problems*, PhD the-
832 *sis*, Universität zu Köln, Germany, 2016.
- 833 [21] A. HEINLEIN, C. HOCHMUTH, AND A. KLAWONN, *Fully algebraic two-level overlapping schwarz*
834 *preconditioners for elasticity problems*, technical report, Universität zu Köln, December
835 2019, <https://kups.ub.uni-koeln.de/10441/>.
- 836 [22] A. HEINLEIN, C. HOCHMUTH, AND A. KLAWONN, *Monolithic overlapping Schwarz domain de-*
837 *composition methods with GDSW coarse spaces for incompressible fluid flow problems*,
838 *SIAM J. Sci. Comput.*, 41 (2019), pp. C291–C316, <https://doi.org/10.1137/18M1184047>.
839 Preprint <https://kups.ub.uni-koeln.de/8355/>.
- 840

- 841 [23] A. HEINLEIN, C. HOCHMUTH, AND A. KLAWONN, *Reduced dimension GDSW coarse spaces for*
842 *monolithic Schwarz domain decomposition methods for incompressible fluid flow prob-*
843 *lems*, International Journal for Numerical Methods in Engineering, n/a (2019), <https://doi.org/10.1002/nme.6258>, <https://onlinelibrary.wiley.com/doi/abs/10.1002/nme.6258>.
844 Preprint <https://kups.ub.uni-koeln.de/8645/>.
845
- 846 [24] A. HEINLEIN, C. HOCHMUTH, AND A. KLAWONN, *Fully algebraic two-level overlapping Schwarz*
847 *preconditioners for elasticity problems*, tech. report, April 2020. Accepted for publication
848 in the proceedings of the ENUMATH 2019 conference. April 2020. Preprint [https://kups.](https://kups.ub.uni-koeln.de/id/eprint/10441)
849 [ub.uni-koeln.de/id/eprint/10441](https://kups.ub.uni-koeln.de/id/eprint/10441).
- 850 [25] A. HEINLEIN, A. KLAWONN, J. KNEPPER, O. RHEINBACH, AND O. B. WIDLUND, *Adaptive gds*
851 *coarse spaces of reduced dimension for overlapping schwarz methods*, technical report,
852 Universität zu Köln, September 2020, <https://kups.ub.uni-koeln.de/12113/>.
- 853 [26] A. HEINLEIN, A. KLAWONN, S. RAJAMANICKAM, AND O. RHEINBACH, *FROSch – A framework*
854 *for parallel Schwarz preconditioners in Trilinos*. In preparation.
- 855 [27] A. HEINLEIN, A. KLAWONN, S. RAJAMANICKAM, AND O. RHEINBACH, *FROSch: A fast and*
856 *robust overlapping Schwarz domain decomposition preconditioner based on Xpetra in*
857 *Trilinos*, tech. report, April 2019. Accepted for publication in the proceedings of the
858 International Conference on Domain Decomposition Methods 25. April 2019. Preprint
859 <https://kups.ub.uni-koeln.de/9018/>.
- 860 [28] A. HEINLEIN, A. KLAWONN, AND O. RHEINBACH, *A parallel implementation of a*
861 *two-level overlapping Schwarz method with energy-minimizing coarse space based*
862 *on Trilinos*, SIAM J. Sci. Comput., 38 (2016), pp. C713–C747, [https://doi.](https://doi.org/10.1137/16M1062843)
863 [org/10.1137/16M1062843](https://doi.org/10.1137/16M1062843). Preprint [http://tu-freiberg.de/sites/default/files/media/](http://tu-freiberg.de/sites/default/files/media/fakultaet-fuer-mathematik-und-informatik-fakultaet-1-9277/2016-04.fertig.pdf)
864 [fakultaet-fuer-mathematik-und-informatik-fakultaet-1-9277/2016-04.fertig.pdf](http://tu-freiberg.de/sites/default/files/media/fakultaet-fuer-mathematik-und-informatik-fakultaet-1-9277/2016-04.fertig.pdf).
- 865 [29] A. HEINLEIN, A. KLAWONN, O. RHEINBACH, AND F. RÖVER, *A Three-Level Extension of the*
866 *GDSW Overlapping Schwarz Preconditioner in Two Dimensions*, Springer International
867 Publishing, Cham, 2019, pp. 187–204, https://doi.org/10.1007/978-3-030-14244-5_10,
868 https://doi.org/10.1007/978-3-030-14244-5_10. Preprint [https://tu-freiberg.de/sites/](https://tu-freiberg.de/sites/default/files/media/fakultaet-fuer-mathematik-und-informatik-fakultaet-1-9277/preprint_2018_04_heinlein_klawonn_rheinbach_roever.pdf)
869 [default/files/media/fakultaet-fuer-mathematik-und-informatik-fakultaet-1-9277/prep/](https://tu-freiberg.de/sites/default/files/media/fakultaet-fuer-mathematik-und-informatik-fakultaet-1-9277/preprint_2018_04_heinlein_klawonn_rheinbach_roever.pdf)
870 [preprint_2018_04_heinlein_klawonn_rheinbach_roever.pdf](https://tu-freiberg.de/sites/default/files/media/fakultaet-fuer-mathematik-und-informatik-fakultaet-1-9277/preprint_2018_04_heinlein_klawonn_rheinbach_roever.pdf).
- 871 [30] A. HEINLEIN, A. KLAWONN, O. RHEINBACH, AND F. RÖVER, *A three-level extension of the gds*
872 *overlapping schwarz preconditioner in three dimensions*, in Domain Decomposition Meth-
873 ods in Science and Engineering XXV, R. Haynes, S. MacLachlan, X.-C. Cai, L. Halpern,
874 H. H. Kim, A. Klawonn, and O. Widlund, eds., Cham, 2020, Springer International Pub-
875 lishing, pp. 185–192. Preprint <https://kups.ub.uni-koeln.de/9017/>.
- 876 [31] M. R. HESTENES, E. STIEFEL, ET AL., *Methods of conjugate gradients for solving linear systems*,
877 Journal of research of the National Bureau of Standards, 49 (1952), pp. 409–436.
- 878 [32] I. J. HEWITT AND C. SCHOOF, *Models for polythermal ice sheets and glaciers*, The Cryosphere,
879 11 (2017), pp. 541–551, <https://doi.org/10.5194/tc-11-541-2017>, [https://tc.copernicus.](https://tc.copernicus.org/articles/11/541/2017/)
880 [org/articles/11/541/2017/](https://tc.copernicus.org/articles/11/541/2017/).
- 881 [33] M. J. HOFFMAN, M. PEREGO, S. F. PRICE, W. H. LIPSCOMB, T. ZHANG, D. JACOBSEN,
882 I. TEZAUER, A. G. SALINGER, R. TUMINARO, AND L. BERTAGNA, *Mpas-albany land ice*
883 *(mali): a variable-resolution ice sheet model for earth system modeling using voronoi*
884 *grids*, Geoscientific Model Development, 11 (2018), pp. 3747–3780, [https://doi.org/10.](https://doi.org/10.5194/gmd-11-3747-2018)
885 [5194/gmd-11-3747-2018](https://doi.org/10.5194/gmd-11-3747-2018), <https://www.geosci-model-dev.net/11/3747/2018/>.
- 886 [34] T. Y. HOU AND X.-H. WU, *A multiscale finite element method for elliptic problems in composite*
887 *materials and porous media*, Journal of Computational Physics, 134 (1997), pp. 169 –
888 189, <https://doi.org/http://dx.doi.org/10.1006/jcph.1997.5682>, [http://www.sciencedirect.](http://www.sciencedirect.com/science/article/pii/S0021999197956825)
889 [com/science/article/pii/S0021999197956825](http://www.sciencedirect.com/science/article/pii/S0021999197956825).
- 890 [35] T. ISAAC, G. STADLER, AND O. GHATTAS, *Solution of nonlinear stokes equations discretized*
891 *by high-order finite elements on nonconforming and anisotropic meshes, with application*
892 *to ice sheet dynamics*, SIAM Journal on Scientific Computing, 37 (2015), pp. B804–B833,
893 <https://doi.org/10.1137/140974407>.
- 894 [36] A. KLAWONN AND L. PAVARINO, *Overlapping Schwarz methods for mixed linear elasticity and*
895 *Stokes problems*, Comput. Methods Appl. Mech. Engrg., 165 (1998), pp. 233–245.
- 896 [37] A. KLAWONN AND L. PAVARINO, *A comparison of overlapping Schwarz methods and block*
897 *preconditioners for saddle point problems*, Numer. Linear Algebra Appl., 7 (2000), pp. 1–
898 25.
- 899 [38] A. KLAWONN AND O. RHEINBACH, *A parallel implementation of dual-primal FETI methods for*
900 *three-dimensional linear elasticity using a transformation of basis*, SIAM J. Sci. Comput.,
901 28 (2006), pp. 1886–1906.
- 902 [39] W. LENG, L. JU, M. GUNZBURGER, AND S. PRICE, *A parallel computational model for three-*

- 903 *dimensional, thermo-mechanical stokes flow simulations of glaciers and ice sheets*, *Communications in Computational Physics*, 16 (2014), pp. 1056–1080, [https://doi.org/10.4208/](https://doi.org/10.4208/cicp.310813.010414a)
 904 [https://doi.org/10.4208/](https://doi.org/10.4208/cicp.310813.010414a)
 905 [cicp.310813.010414a](https://doi.org/10.4208/cicp.310813.010414a).
- [40] W. LENG, L. JU, M. GUNZBURGER, S. PRICE, AND T. RINGLER, *A parallel high-order accurate finite element nonlinear stokes ice sheet model and benchmark experiments*, *Journal of Geophysical Research: Earth Surface*, 117 (2012), <https://doi.org/10.1029/2011JF001962>,
 906 <http://dx.doi.org/10.1029/2011JF001962>,
 907 <http://dx.doi.org/10.1029/2011JF001962>.
- [41] M. PEREGO, A. BARONE, L. BERTAGNA, T. HILBRANDT, M. HOFFMAN, S. PRICE, AND G. STADLER, *A steady-state thermo-mechanical solver for ice-sheet modeling*, *The Cryosphere*, (“in preparation”).
- [42] M. PEREGO, M. GUNZBURGER, AND J. BURKARDT, *Parallel finite-element implementation for higher-order ice-sheet models*, *Journal of Glaciology*, 58 (2012), pp. 76–88, <https://doi.org/10.3189/2012JG11J063>.
- [43] M. RÜCKAMP, A. HUMBERT, T. KLEINER, M. MORLIGHEM, AND H. SEROUSSI, *Extended enthalpy formulations in the ice flow model issm version 4.17: discontinuous conductivity and anisotropic supg*, *Geoscientific Model Development Discussions*, 2020 (2020), pp. 1–18, <https://doi.org/10.5194/gmd-2020-78>, <https://gmd.copernicus.org/preprints/gmd-2020-78/>.
- [44] Y. SAAD AND M. H. SCHULTZ, *Gmres: A generalized minimal residual algorithm for solving nonsymmetric linear systems*, *SIAM Journal on Scientific and Statistical Computing*, 7 (1986), pp. 856–869, <https://doi.org/10.1137/0907058>, <https://doi.org/10.1137/0907058>,
 922 <https://doi.org/10.1137/0907058>,
 923 <https://arxiv.org/abs/https://doi.org/10.1137/0907058>,
 924 <https://arxiv.org/abs/https://doi.org/10.1137/0907058>.
- [45] A. G. SALINGER, R. A. BARTLETT, A. M. BRADLEY, Q. CHEN, I. P. DEMESHKO, X. GAO, G. A. HANSEN, A. MOTA, R. P. MULLER, E. NIELSEN, J. T. OSTIEN, R. P. PAWLOWSKI, M. PEREGO, E. T. PHIPPS, W. SUN, AND I. K. TEZAUER, *Albany: Using component-based design to develop a flexible, generic multiphysics analysis code*, *International Journal for Multiscale Computational Engineering*, 14 (2016), pp. 415–438.
- [46] C. SCHOOF AND I. J. HEWITT, *A model for polythermal ice incorporating gravity-driven moisture transport*, *Journal of Fluid Mechanics*, 797 (2016), pp. 504–535, <https://doi.org/10.1017/jfm.2016.251>, <https://www.cambridge.org/core/article/div-class-title-a-model-for-polythermal-ice-incorporating-gravity-driven-moisture-transport-div/F2EB0C5650440FFAF7899D1A38C9D424>.
- [47] I. K. TEZAUER, M. PEREGO, A. G. SALINGER, R. S. TUMINARO, AND S. PRICE, *Albany/FELIX: a parallel, scalable and robust, finite element, first-order Stokes approximation ice sheet solver built for advanced analysis*, *Geoscientific Model Development*, 8 (2015), pp. 1–24, <https://doi.org/10.5194/gmd-8-1-2015>.
- [48] I. K. TEZAUER, R. S. TUMINARO, M. PEREGO, A. G. SALINGER, AND S. F. PRICE, *On the scalability of the albany/felix first-order stokes approximation ice sheet solver for large-scale simulations of the greenland and antarctic ice sheets*, *Procedia Computer Science*, 51 (2015), pp. 2026–2035.
- [49] T. TRILINOS PROJECT TEAM, *The Trilinos Project Website*.
- [50] R. TUMINARO, M. PEREGO, I. TEZAUER, A. SALINGER, AND S. F. PRICE, *A matrix dependent/algebraic multigrid approach for extruded meshes with applications to ice sheet modeling*, *SIAM Journal on Scientific Computing*, 38 (2016), pp. c504–c532.